Laser cooling in solids: advances and prospects

2016 Rep. Prog. Phys. 79 096401

(http://iopscience.iop.org/0034-4885/79/9/096401)

IOP Publishing Reports on Progress in Physics
Rep. Prog. Phys. 79 (2016) 096401 (23pp) doi:10.1088/0034-4885/79/9/096401

Review

Laser cooling in solids: advances and prospects

Denis V Seletskiy[1,2], Richard Epstein[1,3] and Mansoor Sheik-Bahae[1]

[1] Department of Physics and Astronomy, University of New Mexico, Albuquerque, NM 87131, USA
[2] Department of Physics and Center for Applied Photonics, University of Konstanz, Konstanz 78457, Germany
[3] Thermodynamic Films, LLC, Santa Fe, NM 87505, USA

E-mail: msb@unm.edu

Received 26 April 2015, revised 27 October 2015
Accepted for publication 4 November 2015
Published 3 August 2016

Corresponding Editor Laura Greene

Abstract

This review discusses the progress and ongoing efforts in optical refrigeration. Optical refrigeration is a process in which phonons are removed from a solid by anti-Stokes fluorescence. The review first summarizes the history of optical refrigeration, noting the success in cooling rare-earth-doped solids to cryogenic temperatures. It then examines in detail a four-level model of rare-earth-based optical refrigeration. This model elucidates the essential roles that the various material parameters, such as the spacing of the energy levels and the radiative quantum efficiency, play in the process of optical refrigeration. The review then describes the experimental techniques for cryogenic optical refrigeration of rare-earth-doped solids employing non-resonant and resonant optical cavities. It then examines the work on laser cooling of semiconductors, emphasizing the differences between optical refrigeration of semiconductors and rare-earth-doped solids and the new challenges and advantages of semiconductors. It then describes the significant experimental results including the observed optical refrigeration of CdS nanostructures. The review concludes by discussing the engineering challenges to the development of practical optical refrigerators, and the potential advantages and uses of these refrigerators.

Keywords: laser cooling, optical refrigeration, rare-earth doped crystals, spectroscopy, anti-Stokes fluorescence

(Some figures may appear in colour only in the online journal)

1. Overview

1.1. Introduction

'Temperature' is regarded as a measure of an average kinetic energy of atoms or molecules in a physical system in a state of equilibrium. Heating or cooling of a medium thus is associated with change of this average kinetic energy. Most common refrigeration techniques, for example mechanical coolers, are unconcerned with the atomic picture as they operate with macroscopic or ensemble properties of the systems. 'Laser cooling' on the other hand, is best understood in the microscopic picture, where energy of the system stored in a particular degree of freedom is reduced by the interaction of atoms with light.

Perhaps the most known scenario of laser cooling is Doppler cooling of dilute gases [1], demonstration of which was awarded the Nobel Prize in physics in 1997 [2]. In a dilute gas, atoms (or molecules [3]) are widely separated from one

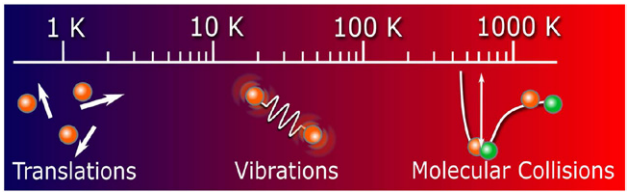

Figure 1. Relevant degrees of freedom, available for laser cooling at various starting temperatures. As discussed in the text, translations are cooled by Doppler effect, coming into play at very low temperatures and highly diluted gases. Redistribution of radiation via molecular collisions can also be utilized for cooling of the translational degrees of freedom in dense and hot gases. Cooling of vibrations through phonon annihilation via anti-Stokes fluorescence is viable in the intermediate temperature range. The latter conditions are typically satisfied in solids and the approach is optical refrigeration of solids.

another, allowing them to move long distances effectively unperturbed by collisions with their neighbors. When cooled, the kinetic energy of the gas stored in the translational degrees of freedom of the constituents is reduced via interaction of the Doppler-shifted atomic transitions with counter-propagating laser beams. Appropriately tuned coherent optical field generates an effective viscous drag ('optical molasses' [4]), thus slowing down the atoms to velocities consistent with temperatures of 1 μK or below. In order to achieve such low temperatures, it is necessary to maintain minimal atomic interactions, and therefore typical atomic densities are $<10^{13}$ atoms cm^{-3}. These densities allow for novel exploration of fundamental physics, such as Bose–Einstein condensation (2001 Nobel Prize in physics) [5], but otherwise have limited practical applications.

At high atomic densities, many-body interactions can no longer be excluded. Despite this fact, the physical picture of laser cooling remains essentially the same. For instance, laser cooling can also be achieved in a dense mixture of hot gases of Rubidium atoms and noble buffer, where collisions result in instantaneous lowering of the Rb transition energy [6, 7]. Coherent laser field, red-detuned from the unperturbed Rb transition becomes resonantly absorbed only during collisions. The absorbed energy is returned to the photon field via an isotropic fluorescent emission at a frequency of unperturbed transition, thus removing energy in the process. In contrast to Doppler cooling of dilute gases, this laser cooling scheme relies on collisional redistribution of radiation in dense and hot interacting gases, however the working principles are nearly the same, as laser light is used to lower energy in the translational degree of freedom via intermolecular interactions. In contrast to Doppler cooling, however, this process does not depend on the recoil momentum in the atom-photon interaction and consequently on the directionality (or counter-propagating nature) of the cooling laser beams.

At moderate temperatures, when cohesive energy of the interparticle interactions is strong enough, a rich plethora of condensed-matter physics phenomena modifies the details of light-matter interaction substantially. In a solid, atomic density is on the order of 10^{23} atoms cm^{-3}, forcing intimate atomic interactions. In this intermediate temperature range of 10–400 K (figure 1), thermal energy of the system is primarily stored in the quanta of the vibrational degrees of freedom, i.e. in the phonons. An example of this system is a transparent host doped with ions having a dipole-active ground-state transition. In this picture, laser energy $h\nu$ is initially deposited into the lowest-energy E_g of the ion. The electrons then thermalize with the environment by absorbing host phonons and carry that energy out of the system through higher energy radiation at $h\nu_f$; i.e. anti-Stokes fluorescence. Thus, the simplified cooling efficiency η_c of the process can be expressed as [8]:

$$\eta_c = \frac{h\nu_f - h\nu}{h\nu} \approx \frac{k_B T}{E_g}, \tag{1}$$

where k_B is the Boltzmann constant and T is the temperature. A typical cooling efficiency is on the order of a few percent at room temperature for $E_g \sim 1$ eV. This efficiency is in the practical range, as compared with 10^{-6} efficiency of Doppler cooling [9]. Cooling by annihilation of phonons through anti-Stokes fluorescence is typically given names 'optical refrigeration' or 'laser cooling of solids'. Anti-Stokes fluorescence cooling is not limited to solids, having been reported in liquids [10], and gasses [9]; the latter, in fact, is regarded as the first demonstration of net fluorescence cooling in matter. Solids, however, are of interest due to the wide variety of possible solid-state cooling applications. For the purpose of this review, any reference to laser cooling or optical refrigeration will be in the context of solids unless otherwise explicitly stated. This review focuses on the laser cooling of solids, highlighting historical developments, experimental progress toward cryogenic optical refrigerators, prospects for emerging applications and a list of outstanding challenges in this rapidly growing field. As will be reviewed below, novel applications are emerging at a time when cryogenic cooling to sub-100 K [11, 12] is routinely demonstrated in ytterbium doped yttrium lithium fluoride crystals.

Most modern cooling applications use mechanical refrigerators, typically consisting of vapor-compression, vapor-absorption and gas-cycle refrigerators. Mechanical refrigerators use a working fluid to absorb and reject heat in a closed cycle. Exploiting the Joule–Thompson effect, these refrigerators were the first to reach cryogenic temperatures in the late 19th century. Advancements in cryogenic refrigeration led to the discoveries of superconductivity and superfluidity, and have enabled a wide range of new applications.

In particular, many semiconductor based detectors benefit from cryogenic operation. The electron-multiplying charge-coupled device (EMCCD), for example, becomes 10-fold more sensitive at −70 °C than at room temperature. Other detectors which benefit from cooling include HgCdTe and InSb, which are used for sensing of long-wave (8–12 μm) and mid-wave (3–5 μm) infrared (IR) light [13] as well as high-purity germanium (HPGe), used for high-resolution gamma-ray spectroscopy [14]. These materials detect light when incident photons excite an electron from the valence band to the conduction band inducing a measureable current. For weak signals and before the onset of unavoidable quantum-limited shot-noise, the statistics of the detected current is typically affected by the parasitic 'dark' currents, resulting

from thermal fluctuations in the detector, which also excite electrons. This noise is particularly detrimental for longer wavelength detectors, since the energy gap between the valence and conduction band is small and the corresponding level of interband thermal excitations is exponentially large. Cryogenic cooling of the detectors is thus necessary to reduce the thermal noise and to ensure optimal sensitivities.

Practical complications may arise when cooling semiconductor detectors using mechanical cryocoolers in applications with strict size, mass, power and stability requirements such as space-based or airborne deployment. A particular drawback of such cryocoolers is microphonic vibration and wear caused by the moving parts. Optical refrigeration of solids elegantly overcomes these drawbacks, as heat is removed optically and no moving parts are required. Solid-state refrigerators, including optical and thermo-electric coolers (TECs) are inherently vibration-free, compact with no moving parts, offering distinct advantages over their mechanical counterparts. TECs are based on the Peltier effect, where an electric current drives a heat flux away from the junction of two different materials, moving heat from one side of the device to the other. Unfortunately, performance of current TECs is limited to cooling to absolute temperatures above around 175 K, higher than the operating temperature of many deployed detectors and high-temperature superconductors. While recent proposal utilizing transverse Peltier effect in thin films is encouraging for low temperature TEC operation [15] at the moment however, optical refrigeration with the current temperatures <100 K remains the only feasible cryogenic solid-state cooler technology. Additionally, a study by Ball Aerospace Corporation showed that rare-earth-based optical refrigeration can outperform conventional thermoelectric and mechanical coolers for low-power, space-borne operations in the 80–170 K temperature range [16]. Finally, optical refrigeration in solids is currently the only viable approach for potential spot-cooling of microscale and nanoscale electronics.

1.2. Historical development

The idea of optical refrigeration was conceived well before the invention of the laser, but was not accepted without controversy. During the 19th century, it was believed that light emitted by a source must always be red-shifted, or equivalently emit at longer wavelengths, as compared to the light absorbed by that source. This was reasoned from the viewpoint of conservation of energy, further verified by experiences that light shining on a material induced heating. The so-called 'Stokes' law' stated that: 'the rays emitted by a fluorescent substance *always* have a smaller refrangibility than the exciting rays' [17], where the refrangibility, which is related to light's refraction, is equivalent to photon energy in this context. By the beginning of the 20th century, observations of anti-Stokes radiation refuted the 'Stokes' law' and in 1929, Pringsheim suggested the possibility of using the anti-Stokes fluorescence process to cool a fluorescent gas with radiation [18]. This proposal was initially deemed controversial as it was believed to violate the second law of thermodynamics [19]. Pringsheim's ideas were put onto a firm theoretical footing in 1946, when Landau formally assigned entropy to light [20]. The second law states that entropy of an isolated system cannot decrease. Landau pointed out that entropy of the radiation field is a function of both the solid angle of the propagating light and the frequency bandwidth, such that both of these properties have to increase during anti-Stokes fluorescent cooling. In other words, optical cooling is possible when a coherent laser source of low-entropy light with narrow spectral bandwidth and high directionality is converted into a broadband, isotropic luminescence, increasing entropy of the system in the process, even in the presence of local cooling. At this point, it is interesting to point out a formal analogy of a laser to a quantum heat engine [21], which transfers photon energy from the incoherent (high 'temperature') pump field to a cold reservoir of high-coherence output. Therefore, a reversed process corresponds to a refrigeration cycle. Laser cooling processes involving photons resonant to a characteristic transition in a system are formally analogous to a situation of a laser running in reverse [22, 23].

As will be discussed in detail below, optical cooling via anti-Stokes fluorescence requires transitions with high quantum efficiency. In the 1950s Kastler [24] and Yatsiv [25] proposed the use of rare-earth (RE) ions doped in transparent solids. There, screening of 4f electrons by higher shells is advantageous for reduction of non-radiative processes [23, 26]. After the invention of the laser in the 1960s, the first attempt to cool a solid was performed by Kushida and Geusic of Bell Telephone Laboratories in 1968 using an Nd^{3+}:YAG crystal [27]. Although the crystal heated, they observed reduced heating as compared with an undoped YAG crystal, leading to the conclusion that heating from impurities was more dominant than the cooling process.

In 1995 Epstein and co-workers at Los Alamos National Laboratory observed the first net cooling of Yb^{3+}-doped ZBLANP (ZrF_4–BaF_2–LaF_3–AlF_3–NaF–PbF_2) glass [8]. In addition to high-quantum efficiency, this host was ideally suited from the material purity requirements benefitting from the developments by the telecommunications industry of low-loss optical fibers in the near-infrared [28]. Throughout the years, cooling has been observed in a number of materials, including Yb^{3+} doped hosts: ZBLANP [8, 29–31], ZBLAN [32–36], ZBLANI [37], CNBZn [38, 39], BIG [34, 40], $KGd(WO)_4$ and $KY(WO)_4$ [41], YAG [41–43], Y_2SiO_5 [42], KPb_2Cl_5 [42], BaY_2F_8 [44, 45], YLF [46–48], ABCYS [49]; Tm^{3+} doped ZBLAN [50, 51], BYF [52] and YLF [53]; Er^{3+} doped CnBZn [54] and KPb_2Cl_5 [54, 55] and Ho^{3+}:YLF [53]. Other reviews can also be consulted for additional details [23, 26, 41, 56, 57, 59, 60]. In 2005, experimental efforts have culminated with cooling of highly purified Yb^{3+}:ZBLAN glass to 208 K from room temperature [31]. Following realization of large resonant enhancement of cooling performance in crystal hosts [48], cryogenic optical refrigeration was achieved in ytterbium-doped fluoride crystals (Yb^{3+}:$YLiF_4$) to a temperature of 114 K starting from 300 K [61, 62]. Most recent results from the University of New Mexico team report cooling to 91 K of a 10 mol% Yb^{3+}-doped $YLiF_4$ crystal [11, 12]. This final temperature is near the minimum achievable temperature of the most pure materials that are currently

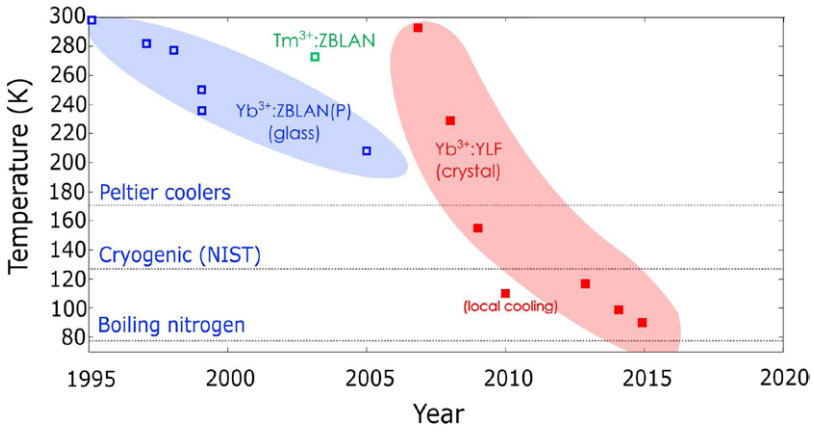

Figure 2. Historical development summarizing experimental progress toward low temperature operation of RE-doped optical refrigerator. Dramatic improvement in performance is evident for transition between amorphous and crystalline host materials. Each point (open and closed squares) represent an experimental result, reported in references contained in this review. Peltier limit and cryogenic barrier (as defined by National Institute for Standards and Technology) have been recently surpassed, and boiling point of liquid nitrogen is within experimental reach in a foreseeable future.

available. Cooling to 91 K is a milestone in the development of optical cryocoolers and a major step toward achieving a liquid nitrogen operation point (figure 2).

Further theoretical and experimental studies have considered laser cooling via spontaneous and stimulated Raman scattering [63–66], superradiance [67, 68], ferroelectric host [69] and cooling in the nanocrystals [70–73] and oxyfluoride glasses [74, 75]. In addition, electroluminescent cooling [76] and radiative cooling [77] are also being explored. Radiation-balanced lasers [78] have been demonstrated, and athermal lasers and amplifiers co-doped with the RE-ions have been proposed [79, 80]. All-fiber approaches to laser cooling have also been considered [81–83]. Laser cooling in semiconductors is reviewed in detail in the following sections below.

It should also be noted that in systems of high symmetry and strong geometric confinement (for example whispering gallery mode resonators), vibrational modes exhibit quantization effects and a departure from the 'continuum' phonon dispersion, as compared to a bulk material. As a result, it is possible to optimize interaction of light with individual highly-confined mechanical modes [84–87]. Laser cooling in this context refers to lowering of the kinetic energy of a particular mechanical mode only, thus resulting in single-mode cooling, with effective mode temperatures reaching values considerably below the bath (bulk) temperature and even to the quantum ground state [88]. This interesting work is outside the scope of the present review and the reader is referred to a recent review for more information [89].

1.3. Scope of this review

This review focuses on bulk optical refrigeration. In the context of solid-state refrigerators, the best performance to date has been accomplished utilizing the Yb^{3+} rare-earth (RE) ions (section 2); however other trivalent RE ions have also been cooled. Both Tm^{3+} and Er^{3+} have been shown to cool [50–52, 55, 90], pumping at first excited state transitions at 2 μm and 1.5 μm, respectively. Unlike the single 4f electronic state in Yb^{3+}, both thulium and erbium have multiple transition levels available for pumping, so it is also possible to utilize a higher energy transition for cooling [50, 52]. There are advantages for each of the different cooling ions, some of which will be discussed below. In parallel to the work on RE-doped materials, optical refrigeration was also pursued in semiconductors, fueled by the promise of much lower achievable temperatures. The experimental progress in this field has been recently marked by exciting developments of first demonstration of optical refrigeration in II–VI CdS nanobelts [91], cooling in organic-inorganic lead-halide perovskites [92] and record-high external quantum efficiency in III–V semiconductors [93]. Theoretical and experimental progress in this field is reviewed in section 3. Device considerations and emerging applications are discussed in section 4 and the review is concluded with a summary of current challenges and prospects in the field (section 5).

2. Optical refrigeration in rare-earth-doped solids

2.1. The 4-level model for optical refrigeration

The cooling cycle for a typical rare-earth ion involves transition between ground state and excited manifolds containing multiple levels. As a consequence of crystal field created by the electric charges of neighboring ions in the solid host, the $(2J + 1)$-fold degeneracy of each manifold is partially lifted via the Stark effect, leading to $(2J + 1)/2$ levels where J is the total angular momentum. The remaining factor of 2 in degeneracy is due to Kramers theorem on half-integer total spins and is lifted only in the presence of a magnetic field. Consider, for example, the Yb^{3+} ion, which is the most common dopant in optical refrigeration experiments. The crystal field splits the $^2F_{7/2}$ ground state and $^2F_{5/2}$ excited states into manifolds containing 4 and 3 levels respectively as shown in figure 3(a). The most efficient cooling cycle involves laser excitation between E4–E5 followed by thermalization within each manifold and the ensuing fluorescence involving 12 transitions between the Stark levels as shown.

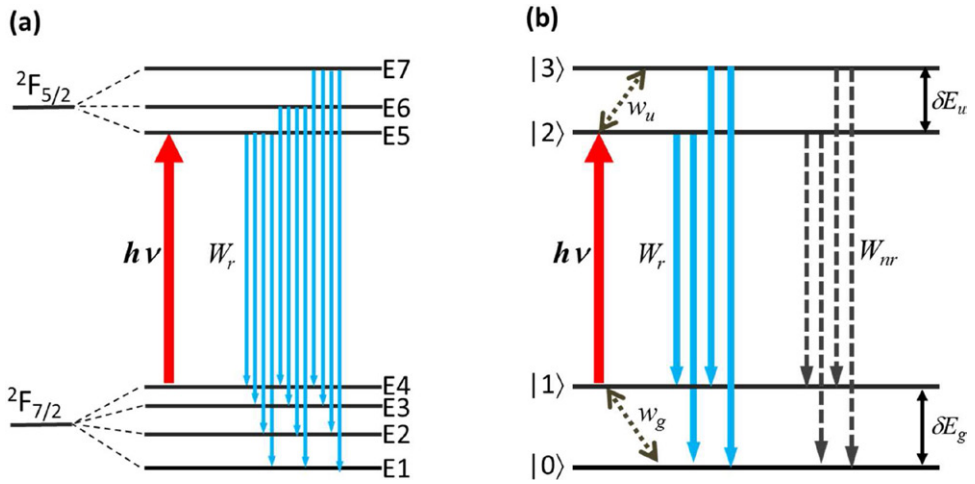

Figure 3. (a) Energy level structure of Yb^{3+} resulting, after partially lifted degeneracy, in 7 levels forming ground (E1–E4) and excited (E5–E7) state manifolds. Optical excitation at a frequency $h\nu$ corresponding to the E4 → E5 transition and possible radiative relaxation pathways with a total rate W_r are depicted with up and down arrows, respectively. (b) The simplified four-level model for optical consisting of two pairs of closely spaced levels: |0> and |1> in the ground state and |2> and |3> in the excited state manifolds.

It is important to note that the energy-level diagram in figure 3 implies zero Stokes shift, as is typical of 4f electrons in a rare-earth ion, e.g., the E4 → E5 absorption occurs at essentially the same energy as the corresponding E5 → E4 emission. The absence of a Stokes shift allows the electronic energy levels to be represented by horizontal lines with no dependence on a configurational coordinate.

To elucidate the essential roles that the various material parameters play in the process of optical refrigeration, it is highly instructive to introduce a simplified 4-level model that will be generally applicable to any such two-manifold cooling system. As shown in figure 3(b), this model involves a two-level ground state having a separation that represents the width of the ground-state manifold δE_g, and similarly, a two-level excited state having an energy splitting corresponding to the width of the excited state manifold δE_u. The laser excitation is assumed to take place between levels 1 and 2 ($h\nu = E_2 - E_1$). The electron–phonon interaction, albeit weak for the 4f electrons in the rare-earth ions, establishes Boltzmann quasi-equilibrium within each two-level manifold on a relatively fast (picoseconds to nanoseconds) timescale with corresponding rates given by w_g and w_u. The excitation then decays into ground state by radiative (solid downward arrows) and nonradiative (dotted downward arrows) relaxations with the corresponding rates of W_r and W_{nr} which are much smaller than the thermalization rates $w_{g,u}$. Following these assumptions, we construct a set of rate equations governing the density populations N_0, N_1, N_2 and N_3:

$$\frac{dN_1}{dt} = -\sigma_{12}\left(N_1 - \frac{g_1}{g_2}N_2\right)\frac{I}{h\nu} + \frac{R}{2}(N_2 + N_3) - w_g\left(N_1 - \frac{g_1}{g_0}N_0 e^{-\delta E_g/k_B T}\right) \tag{2a}$$

$$\frac{dN_2}{dt} = \sigma_{12}\left(N_1 - \frac{g_1}{g_2}N_2\right)\frac{I}{h\nu} - RN_2 + w_u\left(N_3 - \frac{g_3}{g_2}N_2 e^{-\delta E_u/k_B T}\right) \tag{2b}$$

$$\frac{dN_3}{dt} = -RN_3 - w_u\left(N_3 - \frac{g_3}{g_2}N_2 e^{-\delta E_u/k_B T}\right) \tag{2c}$$

$$N_0 + N_1 + N_2 + N_3 = N_t \tag{2d}$$

where $R = 2W_r + 2W_{nr}$ is the total upper state decay rate, σ_{12} is the absorption cross section associated with $|1> - |2>$ transition, I is the incident laser irradiance and the g_i terms represent degeneracy factors for each level. The weighting factor in the electron–phonon interaction terms (w_u and w_g) maintains the Boltzmann distribution among each manifold at quasi equilibrium. The net power density deposited in the system is the difference between absorbed and out-radiated contributions:

$$P_{net} = \sigma_{12}\left(N_1 - \frac{g_1}{g_2}N_2\right)I - W_r[N_2(E_{21} + E_{20}) + N_3(E_{31} + E_{30})] + \alpha_b I, \tag{3}$$

where the first term is the laser excitation ($|1> - |2>$ transition) and second term includes the spontaneous emission terms from levels |2> and |3> with their respective photon energies. We have also included a term that represents parasitic absorption of the pump laser with an absorption coefficient of α_b. It is straightforward to evaluate the steady-state solution to the above rate equations by setting the time derivatives to zero. For simplicity, we further assume equal degeneracy (as in spin degeneracy $2S + 1 = 2$) for all four levels thus eliminating the g-ratio terms. The set of equations in (2) can be solved to obtain the steady-state population in each level in terms of laser intensity and the given material parameters. We first obtain the absorption of the pump laser and its saturation behavior (assuming homogenously-broadened vibronic levels) in the usual manner:

$$\alpha = \frac{\alpha_0}{1 + I/I_s}, \tag{4}$$

where

$$\alpha_0 = \sigma_{12} N_t \frac{e^{-\delta E_g/k_B T}}{1 + e^{-\delta E_g/k_B T}}, \quad (5)$$

and

$$I_s = \frac{h\nu_{12} R}{\sigma_{12} Z_{gu}}, \quad (6)$$

with $Z_{gu} = 1 + \frac{e^{-\delta E_g/k_B T}(1 + e^{-\delta E_u/k_B T})}{1 + e^{-\delta E_g/k_B T}} \approx 1 + e^{-\delta E_g/k_B T}$. The net power density in (3) can be expressed as:

$$P_{net} = \alpha I \left(1 - \eta_q \frac{h\nu_f}{h\nu}\right) + \alpha_b I, \quad (7)$$

where $\eta_q = (1 + W_{nr}/W_r)^{-1}$ is the (internal) quantum efficiency and $h\nu_f$ denotes the mean fluorescence energy of the four-level system given by:

$$h\nu_f = h\nu + \frac{\delta E_g}{2} + \frac{\delta E_u}{1 + (1 + R/w_u) e^{\delta E_u/k_B T}} \quad (8)$$

Despite its simplicity, the four level model reveals essential features of solid-state optical refrigeration. First, equation (5) exhibits diminishing pump absorption due to thermal depletion of the top ground state at low temperatures, $k_B T < \delta E_g$. This implies that the width of the ground-state manifold (δE_g) must be narrow to achieve cooling at low temperatures with reasonable efficiency, as is often the case for ytterbium ions in fluoride host materials. This issue will be revisited when discussing semiconductors in section 3. Second, equation (8) shows that the mean fluorescence photon energy is red shifted at low temperatures, which further lowers the cooling efficiency. This shift would be enhanced if the electron–phonon interaction rate (w_u) is smaller than the upper state recombination rate (R). This means that if $w_u < R$, decay of the excited state can occur before thermalization with the lattice, which results in less fluorescence upconversion and less cooling [94]. This extreme limit of *cold electron recombination* is an issue for semiconductors at very low temperatures where the electrons interact with the lattice primarily via the low-energy and hence relatively slow acoustic phonons [95]. In RE-doped systems, however, $R \sim W_r \sim 10^3$ s^{-1} signifying the small oscillator strengths associated with the dipole-forbidden 4f–4f transitions. The radiative rates are also nearly independent of lattice temperature. Recall that the shielded 4f electrons have also a weak electron–phonon coupling thus $w_{u,g}$ are not as large as their counterparts in transition metals or semiconductors. By contrast, their strength depends on the phonon population number and is therefore strongly temperature dependent. Spin-lattice relaxation times of ~5 ps at 300 K, 60 ps at 140 K and up to nanoseconds at 50 K as reported in [96] are nonetheless shorter than radiative lifetimes by many orders of magnitude; thus rendering $R/w_{g,u} \ll 1$ in all cases.

Dividing the equation (7) by the total absorbed power density $P_{abs} = (\alpha + \alpha_b)I = \eta_{abs}$ gives the cooling efficiency $\eta_c = -P_{net}/P_{abs}$:

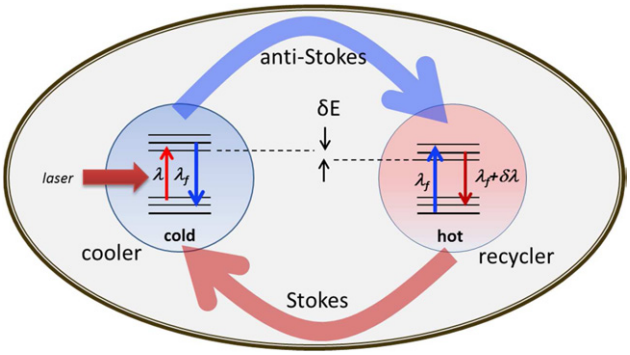

Figure 4. Principle of optical converter. The pump laser light is blue-shifted into waste fluorescence by the cooling elements. The recycling material redshifts this light so that it increases the cooling power when it is reabsorbed by the cooling element.

$$\eta_c = \eta_q \eta_{abs} \frac{h\nu_f}{h\nu} - 1, \quad (9)$$

which yields the idealized efficiency of equation (1) when $\eta_q \eta_{abs} \to 1$. A useful feature of the 4-level model is its description of the temperature-dependence of the cooling in a physically transparent manner. As the temperature is lowered, red-shifting of mean fluorescence wavelength combined with the reduction of the resonant absorption reduces the cooling efficiency. At temperature $T = T_m$ the cooling stops, i.e. when $\eta_c(T_m) \to 0$. This minimum achievable temperature (T_m) can be lowered by reducing the background absorption (higher purity), increasing the quantum efficiency, and enhancing the resonant absorption or choosing a material with a narrow ground state manifold. The effect of fluorescence trapping and its consequent re-absorption by both resonant and parasitic processes diminishes the quantum efficiency. We will discuss this in detail when we analyze of laser cooling in semiconductors where total internal reflection leads to substantial trapping.

2.2. Efficiency enhancement and thermodynamics of optical refrigeration

The ideal cooling efficiency in an optical refrigerator $\eta_c = (\nu_f - \nu)/\nu \sim k_B T_C/h\nu$ is obtained under the assumption that the thermal energy $h\nu$ is carried away by fluorescence photons having energy $h\nu_f \sim h\nu + k_B T_C$. The thermodynamic foundation of this process was only resolved and accepted once Landau assigned entropy and flux temperature to light. In such a picture, low-entropy stream of photons from a coherent (narrow band and directional) light source (such as a laser) is absorbed, and subsequently upconverted to broadband and omnidirectional fluorescence, thus carrying much higher entropy. Thermodynamic analysis of optical refrigeration has been considered in detail by various authors [97–99]. The cooling efficiency was found to follow a Carnot-type inequality:

$$\eta_c \leqslant \frac{T_C}{T_F - T_C}, \quad (10)$$

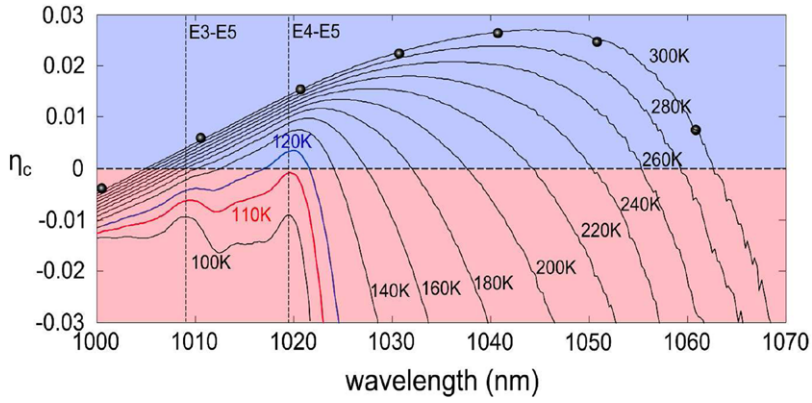

Figure 5. Calculation of cooling efficiency $\eta_c(\lambda)$ spectra of a 5% Yb^{3+}:YLF_4 ($E\|c$ orientation) crystal as a function of temperature, with experimental input parameters $\alpha(\lambda,T)$, $\lambda_f(T)$, $\eta_{ext}(T)$ and $\alpha_b(T)$. The latter two quantities are obtained from the fit (solid line labeled '300 K') of the fractional heating measurements (circles), yielding respective values of $\eta_{ext} = 0.995 \pm 0.001$ and $\alpha_b = (4.0 \pm 0.2) \times 10^{-4}$ cm^{-1}. Calculation assumes temperature-independence of η_{ext} and α_b. The validity of this assumption is verified by independent measurements of the local temperature change [105]. Enhancement of the cooling efficiency at E4–E5 and E3–E5 Stark manifold transitions of Yb^{3+}:YLF_4 are observable at low temperatures. Adapted with permission from [105]. Copyright 2011 OSA.

where T_C is the temperature of the cooling material and T_F the temperature of the fluorescence. In the limit of fluorescence having nearly a black-body behavior, we take $T_F \sim h\nu_F/k_B$ in (equation (10)) which leads to the ideal cooling efficiency. For the typical systems of interests (e.g. a Yb-based cooler at 100 K), this efficiency is ~1%, far lower than the Carnot efficiency of a heat engine given by $T_C/(T_H - T_C)$ where T_H (~300 K) is that of the ambient (hot reservoir). This low efficiency stems from the fact that the fluorescence ($T_F \sim 10^4$ K) that essentially carries the heat and the laser absorbed power is all wasted. Efficiency may therefore be improved by harvesting (recycling) this fluorescence. Two potential schemes can be implemented to accomplish such photon-waste recycling. The first scheme involves exploiting photovoltaic (PV) power converters to capture the fluorescence and convert it to electricity [26, 100]. The enhancement in efficiency can be shown to be $\sim(1 - \eta_{PV}\eta_L)^{-1}$ where η_{PV} and η_L are the electrical efficiency of the PV and laser devices respectively. Interestingly, it was shown that when $\eta_{PV} = \eta_L \sim 1 - k_B T_H/h\nu$, with T_H denoting the temperature of the heat-sink where these devices are held at, the cooling efficiency approaches that of Carnot [26]. With existing high-efficiency PV and laser diode technologies, enhancement factors of 1.5–2 are feasible.

A second scheme for reusing the waste fluorescence employs an all-optical approach where anti-Stokes florescence is down-shifted in another medium and feedback to the cooling medium [101]. Figure 4 describes the principles of this type of optical converter. Absorbing materials in the recycling chamber capture the waste fluorescence and reemit it at redshifted wavelengths. If the absorbing materials are appropriately chosen, the re-emitted light has the required spectrum to produced additional heat removal from the cooling element.

Following a rate-equation analysis that describes the flow of energy (photons) between the laser, the cooling crystal (cold side) and the fluorescence recycle (hot side), we derive (under steady-state conditions) a modified cooling efficiency [102]:

$$\eta_c = \eta_{ext}\frac{\lambda}{\lambda_f}\left(\frac{1 - \gamma(1 - \delta\lambda/\lambda_f)}{1 - \gamma\eta_{ext}}\right) - 1 \qquad (11)$$

Here, for simplicity, we have ignored the parasitic (background) absorption; thus $\alpha_b = 0$ and have explicitly written η_q as external quantum efficiency η_{ext}, the difference arising due to re-absorption and photon trapping, more prevalent in high refractive index materials such as semiconductors, as discussed in section 3. Here we note that the enhanced form of the cooling efficiency resembles equation (9), except for the recycling factor given by the term in the bracket. This factor involves the product of $\gamma = \varphi_1\varphi_2\eta_{ext}^h$ with η_{ext}^h denoting the external quantum efficiency of the recycler, φ_1 = fraction of absorption of anti-Stokes fluorescence in the recycler, and φ_2 = fraction of absorption of the Stokes-shifted fluorescence in the cooling medium. $\delta\lambda$ corresponds to the Stokes shift of the mean fluorescence wavelength in the recycler. For $\eta_{ext} \sim 1$ (the case for Yb:YLF), and assuming the laser detuning is made the same as the Stokes shift ($\lambda - \lambda_f = \delta\lambda$), the overall enhancement defined as $\eta_c(\gamma)/\eta_c(0)$ can be shown to vary as $\sim(1 - \gamma)^{-1}$.

In rare-earth-doped coolers (such as Yb^{3+}) this can be achieved by coating the walls of the cooler's enclosure with high quantum efficiency multiple quantum wells designed to have a mean emission that coincides with the optimum cooling wavelength. Implementing the above scheme, a factor of 2 enhancement ($\gamma \sim 0.5$) could be reachable [102].

2.3. Experimental results on cryogenic optical refrigeration

The main objective of cryocoolers is to reach lowest possible temperatures while maintaining large heat lifts. The first requirement is related to the material purity, as discussed above. The second requirement is addressed by proper heat management and power scaling (i.e. avoidance of saturation, see section 2.1 above). Below we review recent progress in

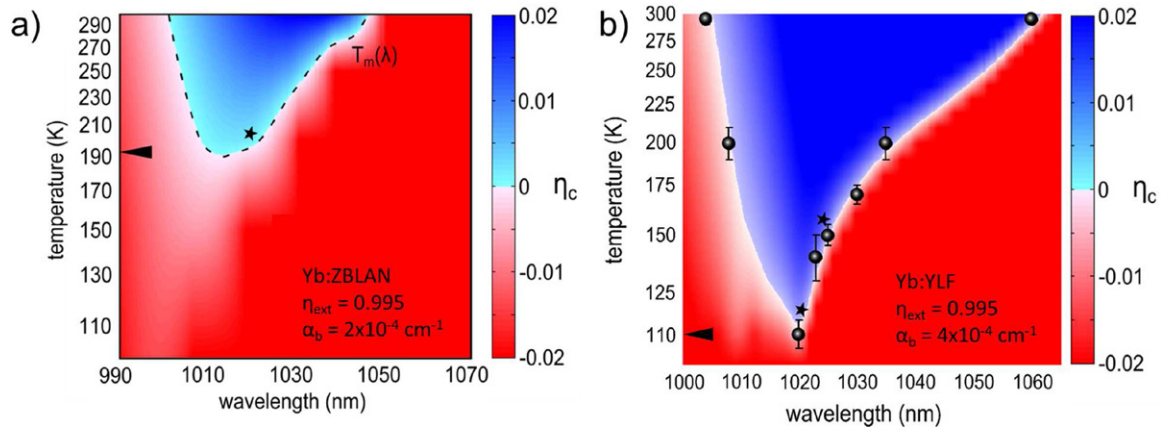

Figure 6. Calculated $\eta_c(\lambda,T)$ for 1% doped Yb:ZBLAN (glass, panel (a)) and 5% doped Yb:YLF (crystal, panel (b)) materials based on experimental input (blue indicates cooling region). Less inhomogeneous broadening of the absorption lines of Yb^{3+} ion doped into the crystalline host is manifested by strong enhancement of the cooling efficiency around 1020 nm, resulting in minimum achievable temperature of 110 K. At the same time, large inhomogeneous broadening in ZBLAN host results in a strong reduction of the resonant enhancement, corresponding to T_m of 190 K around ~1012 nm. In both cases, η_{ext} and α_b have similar values, as indicated. Measurements of the minimum achievable temperature of Yb:YLF as a function of pump wavelength is shown with circles in panel (b). Star-shaped points on both panels indicate several measurements of the bulk cooling performance in the compared material systems. Adapted with permission from [103]. Copyright 2013 Elsevier.

addressing these two requirements in ytterbium-doped systems, from the experimental point of view.

2.3.1. Determination of the minimum achievable temperature T_m. To judge the laser cooling performance of a particular material it is important to determine its minimum achievable temperature, T_m. This quantity, as was described above, sets the lowest possible limit on the temperature that a given material can cool to, and is defined by the condition of $\eta_c(T_m) \rightarrow 0$. In an unsaturated case, the precise value of T_m is therefore a function of four material parameters: $\eta_{ext}(T)$, $\alpha(\nu,T)$, $\alpha_b(T)$ and $\nu_f(T)$ [23, 103]. Experimentally determined values can be used to calculate the cooling efficiency spectra $\eta(\nu,T)$ and therefore the T_m using equation (9). From temperature-dependent emission spectra, absorption spectra $\alpha(\nu,T)$ can be calculated using the detailed balance analysis following McCumber [104] and $\nu_f(T)$ is given by the first moment of the emission spectra. The quantities $\eta_{ext}(T)$ and $\alpha_b(T)$ are obtained from the fractional heating measurements, as explained in detail in section 3. Tracking the temperature change of the sample while varying the pump frequency from above to below the ν_f while maintaining constant pump absorption allows one to extract the two values in question via a model fit via equation (9) (figure 5).

Temperature change can be measured either by photothermal deflection [8] or micro-bolometer array ('thermal camera'). High differential sensitivity of the photothermal deflection measurement does not translate to an absolute accuracy and typically thermal camera is a more reliable measurement however with a drawback that sensitivity drops at lower temperatures. The consequence of this is that the measurement of fractional heating at low temperatures is challenging and therefore minimum achievable temperature (T_m) is typically calculated with room temperature η_{ext} and α_b values. An example of such calculation is depicted in figure 5, where fractional heating measurement is shown as circles and a model fit via equation (9) is shown as a solid curve labeled '300 K'. Using this information together with the spectral data, cooling efficiency spectra are then projected for low temperatures. Upon inspection of the calculated graphs, we note that the lowest temperature for which cooling is possible, i.e. for which $\eta_c > 0$ corresponds to 110 K in figure 5. This occurs at a wavelength of 1020 nm. As the temperature is lowered below approximately 160 K, one observes strong and growing enhancement of the cooling efficiency around wavelengths of 1020 nm and 1010 nm. These features correspond to Yb^{3+} Stark manifold E4–E5 and E3–E5 transitions, respectively [106]. The enhancement in the cooling efficiency comes as a result of long-range order in the crystalline YLF host, where static local electric fields around Yb^{3+} are distributed homogeneously, if compared from site to site [48]. As a result, energy splitting of individual ions remains nearly identical, resulting in appearance of sharp absorption lines for sufficiently low vibronic broadening at low temperatures. From equation (9) it is indeed evident that even for the same material purity, absorption enhancement plays a critical role in enhancement of the cooling efficiency. This point is further exemplified if one compares amorphous and crystalline hosts for the Yb^{3+}. Figure 6 shows calculated cooling efficiencies of Yb^{3+}:ZBLAN and Yb^{3+}:YLF with otherwise similar values of η_{ext} and α_b.

While room temperature $\eta_c(\lambda)$ exhibits similar behavior in both materials, the situation changes drastically at low temperatures. In the case of the glassy host, the Stark manifold splitting in Yb^{3+} is inhomogeneously broadened by site-dependent quasi-random distribution of the local fields, resulting in featureless spectrum of the cooling efficiency and minimum achievable temperature of 190 K. In contrast, η_c in Yb:YLF shows distinct resonant feature at the E4–E5 transition, resulting in T_m of 110 K. It is interesting to point out that while currently E4–E5 transition is the target line for operations down to approximately 70 K, the enhancement in η_c would shift to a shorter wavelength corresponding to the E3–E5 at even lower temperatures. An additional distinct advantage of the crystalline host is in the fact that larger

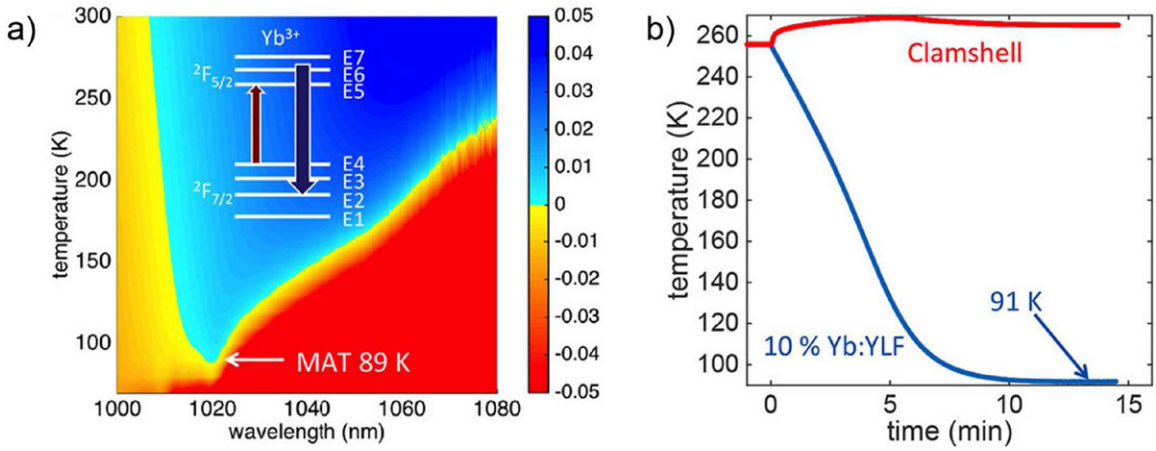

Figure 7. (a) Calculated temperature-dependent spectra of the cooling efficiency for a 10% doped Yb:YLF with $\eta = 0.995$ and $\alpha_b = 10^{-4}$ cm^{-1} with minimum achievable temperature of 89 K. (b) First laser cooling below 100 K, achieved after 15 min of high-power excitation at 1020 nm. The measured temperature is within 2 degrees from the model-predicted minimum achievable of 89 K. The red curve ('Clamshell') depicts a temperature of an actively cooled low-emissivity chamber that surrounds the crystal (adapted with permission from [12]). Copyright 2016 Nature Publishing Group.

doping is stoichiometrically allowed, even further enhancing the resonant absorption. The assumption of nearly temperature independence of η_{ext} and α_b implicit in the above calculations is experimentally validated down to temperatures of about 100 K. Circles in figure 6(b) depict spectrum of the minimum achievable temperature, as measured via a local temperature probe [105]. The locality of the measurement [7, 8, 105, 107] is necessitated by the experimental need of clamping the bulk temperature of the sample via a high-thermal conductivity cold-finger connection. The small and local transient temperature change is acquired by a fast rendition [37, 105, 108] of differential luminescence thermometry (DLT) [48, 109, 110], which is an optical pump-probe temperature measurement technique where calibrated changes in the luminescence lineshape are differentially compared to a reference spectrum, thus gaining sensitivity to small variations in temperature. The measurements fully reproduce the calculated spectrum T_m and in particular the predicted 110 K value, thereby providing experimental validation for the temperature-independent assumption of η_{ext} and α_b. This outlined and relatively simple experimental procedure together with the model of the cooling efficiency (equation (9)), provide an accurate prediction of the cryogenic performance of a given optical refrigeration material. This framework serves as a diagnostic and a verification tool for the ultimate performance of an optical refrigerator. As will be discussed in section 3, the situation is more complicated in semiconductors, due to the intrinsic nonlinearity of the cooling efficiency in carrier density.

2.3.2. Bulk cooling to cryogenic temperatures. For a given laser cooling material, achievement of the minimum possible temperature with largest heat-lift is the primary driver for laser-cooling research and its further transition to real-world applications. Demonstration of an operating temperature of an optical cryocooler prototype near T_m requires careful thermal management considerations, summarized in the expression for temperature evolution [31, 51, 97]:

$$C\frac{dT}{dt} = P_{load}(T) - P_{cool}(\lambda, T), \tag{12}$$

where P_{load} and P_{cool} are the heat load and the cooling power, respectively, and C is the heat capacity of the cooling material. The total heat load has contribution of the radiative, convective and conductive heat loads. The last two contributions are minimized placing the sample in a high vacuum and using low-thermal conductivity supports. The fundamental heating term that remains is the black-body radiative load [90, 97]:

$$P_{thermal} = \frac{\sigma\varepsilon_s A_s}{1+\chi}(T_c^4 - T_s^4), \tag{13}$$

with σ being the Stefan–Boltzmann constant ($\sigma = 5.67 \times 10^{-8}$ W m^{-2} K^{-4}), the chamber and sample temperature of T_c and T_s. To minimize this load, one has to maximize an experimental prefactor $\chi = (1-\varepsilon_c)\varepsilon_s A_s/\varepsilon_c A_c$ where A_j and ε_j (j = s,c) refer to respective surface areas and thermal emissivities of the sample and the chamber. Thus a small chamber around the laser cooling sample covered with a special low-emissivity coating is desirable [31, 90, 111]. The negative contribution on the left hand side of equation (12), P_{cool}, is given by:

$$P_{cool} = \eta_c(\lambda, T)P_0(1 - e^{-N\alpha(\lambda,T)L}), \tag{14}$$

a product of the cooling efficiency and the absorbed power which is given as a product of the laser input power P_0 and the absorbance term in the brackets, which depends on the resonant absorption coefficient α and an effective interaction length NL. For a given material, the strategy to optimize the cooling efficiency is outlined in previous sub-section. The interaction length NL is enhanced by increasing the path of the pump beam through the sample. In practice, this is achieved either via a non-resonant or resonant cavity approaches. In one example of the former, the laser light is admitted through a small hole in the input-coupler of the cavity, containing the cooling element inside [31, 48, 100]. Small misalignment of the pump input with respect to the $TEM_{0,0}$ mode

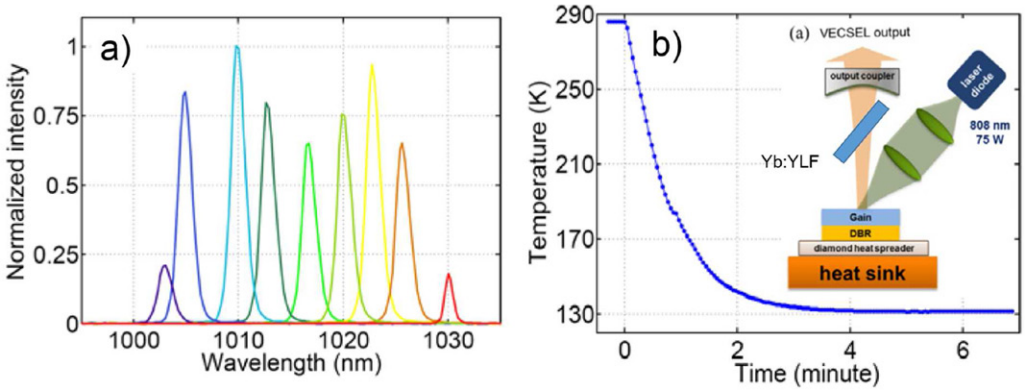

Figure 8. (a) Output tunability of a vertical cavity surface emitting laser (VECSEL), necessary for low-temperature operation of an intra-cavity optical cryocooler. Output powers in excess of 20 W and slope efficiency >40% are demonstrated. (b) Optical refrigeration resulting in a temperature of 131 K, reached by the intra-cavity Yb:YLF cooling element (cavity layout of the laser is shown in the inset, laser cavity is entirely enclosed in a vacuum chamber, not shown). After self-starting lasing action at room temperature, the oscillating wavelength is continuously adjusted via an intra-cavity birefringent filter (not shown), with maximal cooling achieved at 1020 nm. Adapted with permission from [116]. Copyright 2014 OSA.

of the cavity traps pump light for N round-trips [112]. In 2015, the University of New Mexico (UNM) team achieved first cooling below 100 K in a 10% Yb:YLF sample using non-resonant pump trapping scheme together with optimized cooling efficiency (see next sub-section) and thermal load management. The results are shown in figure 7, where calculated minimum achievable temperature (MAT) of 89 K is nearly matched by the measured cooling to 91 K, depicted in panel b. This temperature marks an important milestone in the quest of optical refrigerators to reach the boiling point of liquid nitrogen. Given the effective cross-section of the sample of ~3mm^2, the UNM team achieved excellent trapping with 22 pump passes through the crystal resulting in an absorption of nearly 42% [11, 12].

While the relative ease of use of the non-resonant cavities is advantageous for non-power limited cases, in general resonant cavity approach promises to achieve a more tunable and controlled way of managing intracavity power. A possibility of achievement of nearly 100% intra-cavity absorption via optical impedance matching [113] of a cavity input-coupling mirror to the intra-cavity losses is possible. Resonant cavity experiments have demonstrated nearly 95% total absorbance in the laser cooling sample [114]. Instead of using a 'cold' cavity with only loss term, gain can also be introduced [36, 115]. In this case, interferometric stabilization of the cavity length is not required, since the active cavity automatically adjusts to environmental fluctuations. An elegant solution is to combine a highly robust optically pumped semiconductor laser (OPSL) gain medium and an intra-cavity Yb:YLF cooling element. This approach has been proposed and achieved by the UNM team, reaching absolute temperatures of 131 K (figure 8). This is the lowest temperature achieved via an intracavity cooler to date. The semiconductor gain medium is grown via an MOCVD technique at Sandia National Laboratories in Albuquerque, NM and consists of multiple $In_{0.23}Ga_{0.77}As$ quantum wells with additional strain compensation, carrier confinement and capped by a low-loss AlAs/GaAs DBR mirror [116]. The tunability of the VECSEL demonstrated in figure 8(a) is accomplished via an intra-cavity birefringent element. When placed inside the cavity, the cooling element perturbs the lasing condition by introduction of a wavelength-dependent intra-cavity loss. Therefore, for fixed small-signal gain of the VECSEL chip, birefringent element is required to tune the oscillating condition toward long wavelengths, thus decreasing the loss via lowering of α. Once lasing action commences and crystal temperature decreases, birefringent element is used to continuously tune the output wavelength in order to achieve the optical impedance matching condition in the active cavity: namely maximal intra-cavity loss (predominantly Yb:YLF luminescence) as a function of pump power and output wavelength. For a given doping level, the crystal thickness is preselected to optimally satisfy this requirement. The final temperature is within a few degrees from the estimated minimum achievable temperature of 128 K, a value increased from the nominal 110 K due to saturation of α (equation (4)) [23]. Further experiments are required to more precisely understand the saturation conditions in the laser cooling elements. Cavity mode engineering and power scaling are required to reach even lower temperatures with large heat lifts. Cryogenic operation is only possible when the whole laser is enclosed inside of a vacuum chamber. Hybrid designs where laser cavity is coupled to an external cooling cavity contained in a vacuum chamber might also be implemented in the future.

3.2.3. Optimization of the minimum achievable temperature. As outlined above, the minimum achievable temperature is entirely dictated by the intrinsic and extrinsic material parameters. The former depend on the choice of the host material and the dopant ion. In general, host materials with narrow ground-state manifold are advantageous for low temperature operation, as was discussed above. The choice of active ions is largely driven by the interplay of the increased cooling efficiency with the reduction of the transition energy on the one hand (equation (1)), and the non-radiative losses, on the other [56, 57].

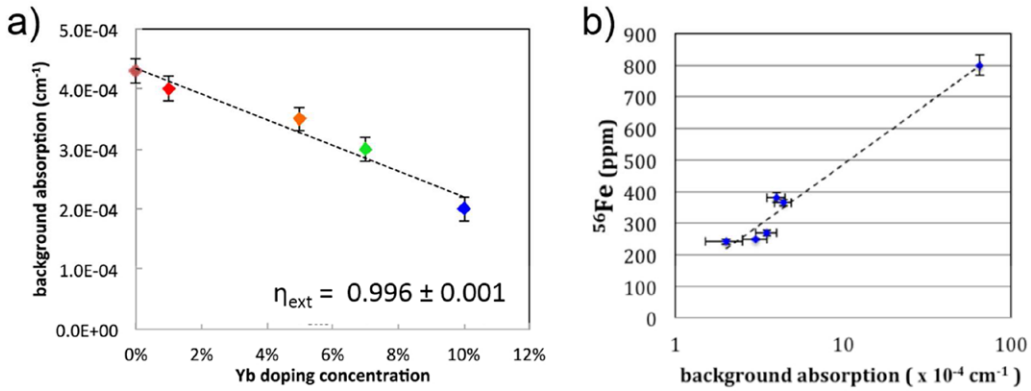

Figure 9. (a) Observed scaling of the background absorption coefficient with increase in Yb^{3+} doping concentration in YLF host in a series of 5 samples, grown back-to-back to decrease potential uncontrolled variations during the crystal growth. Negative slope suggests that impurities are not introduced via the Yb^{3+} during the material synthesis. (b) Elemental analysis obtained with quadrupole inductively coupled mass spectrometer and on the same sample set shows pronounced positive correlation between the background absorption and the measured concentration of iron (Fe). This suggests that iron is the dominant impurity that contributes to the background absorption, in agreement with the modeling conclusions for Yb:ZBLAN in [117]. Adapted with permission from [62]. Copyright 2014 OSA.

Enhancement of the cooling efficiency with the decreased transition energy has been confirmed in Tm^{3+} systems [50, 52]. For a given ion:host systems however, the extrinsic material parameter namely the aforementioned background absorption coefficient α_b is the only experimental variable available for improvement of the cooling performance. Recently, a systematic study of the elemental analysis and laser cooling characterization has been performed on a set of 5 Yb:YLF crystals with increasing Yb^{3+} concentration [62]. Unexpected result showing a decreasing trend of the background absorption with Yb^{3+} concentration yielded record purity performance of a 10% Yb:YLF with $\alpha_b = 10^{-4}$ cm^{-1}. This crystal was in fact used to obtain results in figure 7. The negative trend suggests that impurities are not introduced through the Yb starting powders during the crystal growth procedure. Furthermore, trace element analysis via high resolution mass spectrometry was performed on each sample resulting in observation of positive correlation between the measured background absorption coefficient and iron concentration (figure 9). Similar trend in α_b has been observed in independent studies [118, 119]. While these results require further follow up work, they already provide motivation for selective purification methods of the starting materials in order to lower the background absorption values even lower.

3. Laser cooling in semiconductors

3.1. Overview

Soon after successful observation of net cooling in Yb-doped glass in 1995, attention was directed towards cooling matter in various condensed phases, beyond the rare-earth doped systems. Semiconductors, in particular, have been the focus of numerous theoretical and experimental investigations [120–126]. The impetuses were many including the potential for achieving much lower temperatures than in RE-doped systems (absolute temperatures of 20 K or lower) and the opportunity for direct integration into existing semiconductor-based on electronic and photonic devices. The initial focus was on cooling bulk GaAs double heterostructures [95, 122]. Despite an impressive progress in achieving extremely high external quantum efficiency, net cooling remained elusive due to existence of large parasitic absorption in the band tail [93, 122]. In 2013, however, a team of Singapore researchers took the community by a surprise by reporting direct laser cooling in CdS nanostructures at $\lambda \sim 520$ nm [91]. These results are extremely interesting since II–VI compounds were not known for having the high quantum efficiency required for laser cooling. Demonstration of optical refrigeration in CdS (and potentially other II–VI compounds in the future) has rekindled the interest in laser cooling of semiconductors. Future research to understand these results and investigate their applicability to other compounds will carry great significance.

In the following we present a brief overview of the field by first re-introducing the concept of optical refrigeration in the context of a semiconductor, and point out essential differences, advantages and challenges towards achieving a practical cooling device in this class of materials. We then discuss the significant experimental reports.

The essential difference between semiconductors and RE-doped materials is in their cooling cycles. In the latter, the cooling transition occurs in localized donor ions within the host material while the former involves transition between extended valence and conduction bands of a direct gap semiconductor (see figure 10). Indistinguishable charge carriers following a Fermi–Dirac distribution will allow semiconductors to get much colder than RE materials. As stated earlier, the highest energy levels of the ground state manifold in the RE-doped systems get rapidly depopulated as the temperature is lowered, due to Boltzmann statistics. The cooling cycle becomes ineffective when the Boltzmann constant times the lattice temperature becomes comparable to the width of the ground state (see previous section describing the 4-level model). This sets a practical limit of $T \sim 50$–100 K for most studied RE-doped systems.

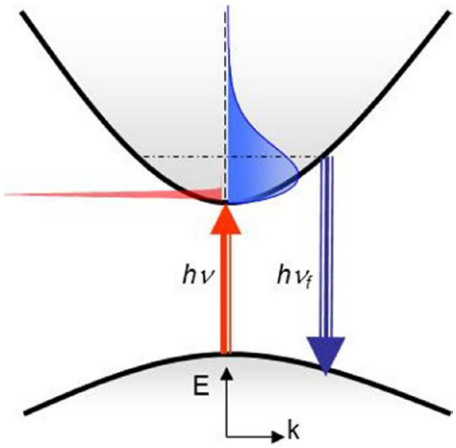

Figure 10. Cooling cycle in laser refrigeration of a semiconductor in which absorption of laser photons with energy $h\nu$ creates a cold distribution of electron–hole carriers (only electron distribution is shown for clarity). The carriers then heat up by absorbing phonons followed by an up-converted luminescence at $h\nu_F$.

Electrons and holes in a clean (undoped) semiconductor, on the other hand, obey Fermi–Dirac statistics, resulting in a full valance band at lattice temperatures below the energy gap. The aforementioned limitation is therefore relaxed as temperatures as low as 10–20 K may be achievable [95, 127]. Semiconductors should also achieve higher cooling power density compared to RE-materials. The maximum cooling power density (rate of heat removal) is $\approx N \times k_B T/\tau_r$, where N is the photo-excited electron (-hole) density and τ_r is the radiative recombination time. In semiconductors the optimal density N is limited due to many-body processes and does not exceed that of moderately doped RE systems. However, we can gain 5–6 orders of magnitude in cooling power density because the radiative recombination rates in semiconductors are much faster than in RE ions [58].

3.2. Theoretical framework

Laser cooling of semiconductors has been examined theoretically [95, 123, 127–135] as well as in experimental studies [26, 92, 93, 126, 139, 136]. A feasibility study by Sheik–Bahae and Epstein outlined the conditions for net cooling based on fundamental material properties and light management [95]. Binder's group at the University of Arizona conducted a comprehensive theoretical study of luminescence upconversion in semiconductor structures. In particular, they presented an elegant microscopic theory of the absorption and luminescence in the presence of partially ionized excitons, which must be understood to attain temperatures approaching 10 K [127, 133]. They also studied the effect of dopants (p- or n-type) in the active (GaAs) or passivation (GaInP) of a double heterostructure [137–139], and analyzed the role of finite spatial distribution of photo-excitation on laser cooing [140]. The role of bandtail states and the possible enhancement of laser cooling by including the effects of photon density of states as well as novel luminescence coupling schemes based on surface plasmon polaritons were investigated in details by Khurgin at Johns Hopkins University [128, 131, 132, 141]. The role of engineering the electronic density of states using quantum confinement (such as multiple quantum wells) were also analyzed [142].

The cooling efficiency in semiconductor materials has been shown to follow the general model of optical refrigeration as represented by

$$\eta_c = \eta_{abs}\eta_{ext}\frac{\nu_f}{\nu} - 1. \tag{15}$$

Here, however, η_{ext} or external quantum efficiency (EQE) is density dependent, unlike in RE-doped systems. This density dependence originates from the various well-known mechanisms for carrier recombination in semiconductors. Of relevance to us, is the equation governing the steady-state e-h density N (in an intrinsic semiconductor) subject to a laser excitation with an average irradiance I [95]:

$$0 = \frac{\alpha(\nu, N)}{h\nu} I - AN - \eta_e BN^2 - CN^3, \tag{16}$$

where $\alpha(\nu,N)$ is the interband absorption coefficient that includes many-body and band-blocking (saturation) factors. The recombination process consists of nonradiative (AN), radiative (BN^2), and Auger (CN^3) rates. All the above coefficients are temperature dependent. The radiative recombination is inhibited by the factor η_e which represents the luminescence escape efficiency. The density-dependence of α can be approximated by [143]:

$$\alpha(N, h\nu) = \alpha_0(N, h\nu)\{f_v - f_c\}, \tag{17}$$

where α_0 denotes the unsaturated absorption coefficient but including the Coulomb screening effects. The strongly density-dependent blocking factor in the brackets contains Fermi–Dirac distribution functions for the valence (f_v) and conduction (f_c) bands. Furthermore, the luminescence escape efficiency is a spectrally averaged quantity:

$$\eta_e = \frac{\int S(\nu)R(\nu)\mathrm{d}\nu}{\int R(\nu)\mathrm{d}\nu}. \tag{18}$$

Here $S(\nu)$ is the geometry-dependent escape probability of photons with energy $h\nu$ and $R(\nu)$ is the luminescence spectral density that is related to the absorption coefficient through reciprocity using a 'non-equilibrium' van Roosbroeck–Shockley relation (also known as Kubo–Martin–Schwinger (KMS) relation) [134, 144, 145]:

$$R(\nu, N) = \frac{8\pi n^2\nu^2}{c^2}\alpha(\nu, N)\left\{\frac{f_c(1-f_v)}{f_v - f_c}\right\}, \tag{19}$$

where c is the speed of light and n is the index of refraction. Note that the radiative recombination coefficient B is obtained by $BN^2 = \int R(\nu)\mathrm{d}\nu$ which results in a negligible dependence of B on N at the carrier densities of interest. Similarly, the mean escaped-luminescence energy $h\tilde{\nu}_f$ defined as

$$h\tilde{\nu}_f = \frac{\int S(\nu)R(\nu)h\nu\mathrm{d}\nu}{\int S(\nu)R(\nu)\mathrm{d}\nu} \tag{20}$$

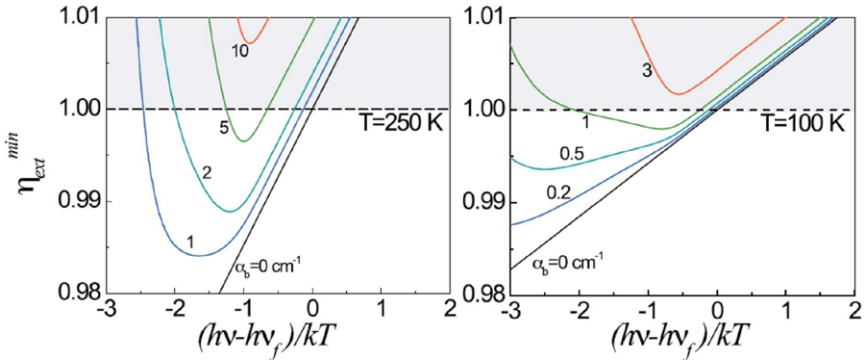

Figure 11. The minimum EQE required to achieve laser cooling versus the normalized excitation photon energy for GaAs at $T = 250$ and 100 K obtained from the inequality of equation (23). The absorption data $\alpha(\nu)$ were obtained by using the KMS relations on the PL spectra on a high quality GaAs/InGaP double heterostructures. Note that for certain background absorption α_b, the requirement $\eta_{ext} > 1$ is unattainable (unphysical) for any wavelength. This restriction becomes more prevalent at lower temperature (used with permission from [26]). Copyright 2009 Wiley.

Note that this quantity can deviate (i.e. redshift) from its internal value ($S = 1$) depending on the thickness or photon recycling conditions.

The density dependent η_{ext} (EQE) follows the recombination rules for an undoped semiconductor:

$$\eta_{ext} = \frac{\eta_e BN^2}{AN + \eta_e BN^2 + CN^3} \approx (\eta_q)^{1/\eta_e} \tag{21}$$

with $\eta_q = BN^2/(AN + BN^2 + CN^3)$ denoting the *internal* quantum efficiency. The approximate equality in equation (21) is valid only for η_{ext} near unity (>0.9). One simple consequence of this relation is that there is an optimum carrier density $N_{op} = (A/C)^{1/2}$ at which η_{ext} reaches a maximum of:

$$\eta_{ext}^{max} = 1 - \frac{2\sqrt{AC}}{\eta_e B} \tag{22}$$

When the parasitic absorption of the fluorescence is also taken into account, it was shown that one should use an effective EQE ($\bar{\eta}_{ext}$) that is reduced from the above value [26]. Similar to RE-doped systems, the practical limitation to lowest achievable temperature or even achieving net cooling is often introduced by the parasitic background absorption in the band-tail as depicted by α_b. We can categorize the possible sources and locations of α_b into three regions: (a) active or core material, (b) cladding layers of the heterostructure, and (c) the substrate, and their heterogeneous interfaces. While situations (b) and (c) can be controlled experimentally by varying the barrier thickness or using high purity substrate respectively, the parasitic absorption from the cooling layer itself presents the most difficult engineering obstacle. It is also instructive to show an alternative and compact way of expressing the cooling condition. With laser excitation at $h\nu < h\nu_f$, the cooling condition of equation (15) ($\eta_c > 0$) reduces to:

$$\eta_{ext} > \frac{\nu}{\nu_f} + \frac{\alpha_b}{\alpha(\nu)} \tag{23}$$

The above inequality emphasizes the critical role of α_b in achieving net laser cooling. The absorption $\alpha(\nu)$ drops sharply for energies considerably below the bandgap, which means this inequality may never be satisfied for any wavelength if α_b is too large. To quantify this argument, we need to know the band-tail absorption accurately. The nature of the band tail states and their dependence on the impurity type and concentration make the reported experimental values very sample-specific. Most theoretical calculations are accurate only for above and near the bandgap wavelengths. It is best to approach the problem experimentally with absorption and luminescence data that allow accurate estimates of the required EQE using equation (23). Starting with the measured low-density photoluminescence (PL) spectrum on a high quality sample, one obtains absorption spectra $\alpha(\nu)$ using the KMS relations of equation (19). The low density approximation reduces the occupation factor to a simple Boltzmann factor, $\exp(-h\nu/k_BT)$, where we ignore possible band-filling (saturation) effects in the band-tail. Using equation (19), the minimum required η_{ext} can be estimated as a function of $h\nu$ for various values of α_b, as depicted in figure 11. Here we assume an extraction efficiency $\eta_e = 0.1$ which is typical of GaAs on a ZnS dome structure. Figure 11 indicates that the required EQE for cooling becomes more demanding as the temperature is lowered which is essentially a consequence of diminishing phonon population at low temperatures. This result mirrors the situation in the rare-earth doped materials. Semiconductors, however, have the fortunate property that their EQE increases with decreasing temperature. The loss terms (A and C coefficients) decrease while the radiative rate (B coefficient) increases inversely with lattice temperature [26, 57, 95].

Another issue of concern is absorption saturation (band-blocking) and many-body interactions. Band-blocking can pose a limiting factor in the bandtail excitation where the density of states is very low [26]. Theoretical models exist that deal with absorption spectra of semiconductor structures under various carrier densities and lattice temperatures. Recently, a rigorous microscopic theory for absorption and luminescence in bulk semiconductors that includes the effects of electron–hole (e–h) plasma density as well as excitonic correlations has been introduced by Rupper *et al* under the quasi-thermal equilibrium approximation [137]. Khurgin has presented simple yet intuitive analysis of the phonon-assisted band-tail

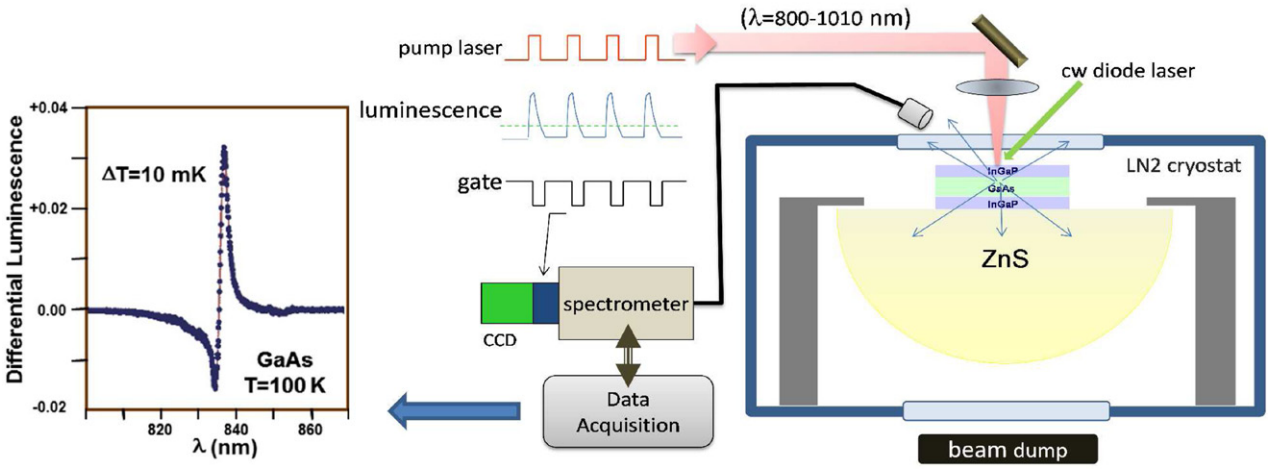

Figure 12. Experimental setup for measuring the external quantum efficiency (EQE or η_{ext}) at various lattice temperatures in GaAs/GaInP double heterostructures. A tunable cw laser (Ti:sapphire, 4.5 W) excites a constant density of electron–hole pairs as the pump is tuned near the band edge. This is done by keeping the luminescence intensity (within a certain spectral band) constant using the monochromator. After recombination is complete, the temperature change of the sample is measured using a time-gated differential luminescence thermometry (TG-DLT) where the spectral shift of the low density luminescence spectrum induced by a weak cw laser diode is monitored using the gated spectrometer. The inset figure shows a typical DLT signal for $\Delta T = 10$ mK in GaAs at $T = 100$ K.

states and the role of band-blocking using a density-matrix approach [131]. These theories all point out the significance of the excitation wavelength in the presence of band-blocking (saturation) which tends to diminish the cooling efficiency predominantly for $T \leqslant 100$ K.

3.3. Experimental work on optical refrigeration in semiconductors

The first thorough experimental effort was reported by the University of Colorado [124]. No net cooling was achieved, despite realization of an impressive external quantum efficiency of 96% in GaAs. These experiments used a high quality GaAs heterostructure optically-contacted to a ZnSe dome structure for enhanced luminescence extraction. A report of local cooling in AlGaAs quantum wells by a European consortium was later attributed to misinterpretation of spectra caused by Coulomb screening of the excitons [146]. The UNM team also focused on GaAs/GaInP double heterostructure and performed numerous experiments to examine the role of thickness and temperature on EQE [26, 93, 110, 147–150].

The samples used in these experiments were made using highly controlled epitaxial growth techniques such as metal organic chemical vapor deposition (MOCVD). This involves a double heterostructure of GaAs/GaInP where the lattice-matched cladding layers provide surface passivation as well as carrier confinement. To deal with extraction efficiency, geometric coupling schemes such as nearly index-matched dome lenses have been employed to enhance η_e to 15%–20%. The double heterostructures were lithographically patterned into ≈1 mm diameter disks, lifted off from their parent GaAs substrates, and then van der Waals bonded to a ZnS dome. The EQE of each sample were measured using the technique of all-optical scanning laser calorimetry (ASLC) at various temperatures and laser pump powers. The experimental setup is shown in figure 12. It employs a novel time-gated differential luminescence thermometry (TG-DLT) to accurately measure the temperature change ΔT induced by a tunable laser in the vicinity of the bandgap of GaAs. The time-gated capability assured that only the long-lived thermally induced changes to the luminescence are measured after the carriers decay in <100 ns.

The pump laser is CW Ti:sapphire laser producing up to 4.5 W tunable in the wavelength range 750–900 nm. This laser is pumped by an 18 W laser at 532 nm (Verdi, Coherent Inc.). The temperature change in the sample is proportional to the net power deposited which can be shown to follow:

$$\Delta T(\nu) \propto P_{\text{lum}}\left(\frac{1}{\eta_{\text{ext}}\eta_{\text{abs}}}\frac{\nu}{\nu_{\text{f}}} - 1\right) \tag{24}$$

where κ is the total thermal conductance (W/K) of the system positioned in an optical cryostat, and $P_{\text{lum}} = h\nu_{\text{f}}\,\eta_e BN^2$ defines the spectrally-integrated luminescence power exiting into free space. It is evident from equation (24) that by keeping P_{lum} constant, the measured ΔT versus photon energy $h\nu$ follows the (linear) energy dependence in the cooling (or heating) regimes. At short wavelengths ($\nu > \nu_{\text{f}}$) where $\alpha(\nu)$ is large, η_{abs} can be taken as unity for moderate to high purity samples, and the fractional heating data follows a straight line $\Delta T(\nu) \propto \frac{1}{\eta_{\text{ext}}}\frac{\nu}{\nu_{\text{f}}} - 1$. Up to date, available GaAs samples do not possess sufficient purity to make this term negative constituting net cooling. When the pump wavelength λ is tuned close to λ_{f}, α_{abs} tends to degrade, thus preventing net cooling. Extrapolation of the short wavelength data has been used to obtain a 'zero-crossing energy ν_c from which $\eta_{\text{ext}} = \nu_c/\nu_{\text{f}}$ can be deduced as depicted in figure 13 for one of the GaAs/GaInP DHS samples at 200 K [110].

The optimum GaAs thickness is found to be about 1 μm, determined by balancing excessive luminescence re-absorption

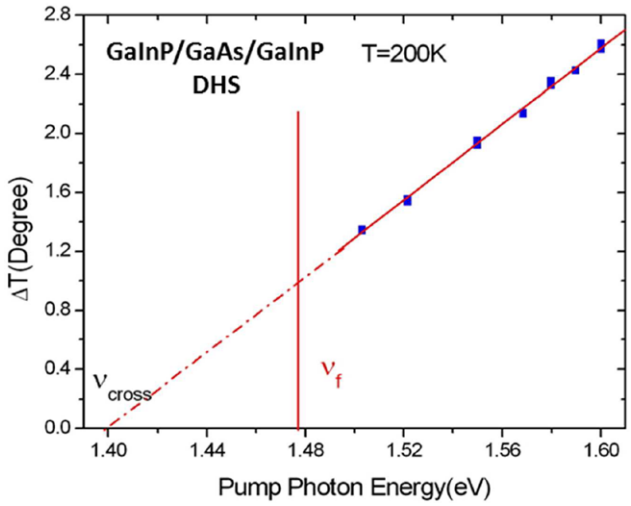

Figure 13. Differential heating data obtained by ASLC method for measuring the external quantum efficiency. Adapted with permission from [110]. Copyright 2011 AIP.

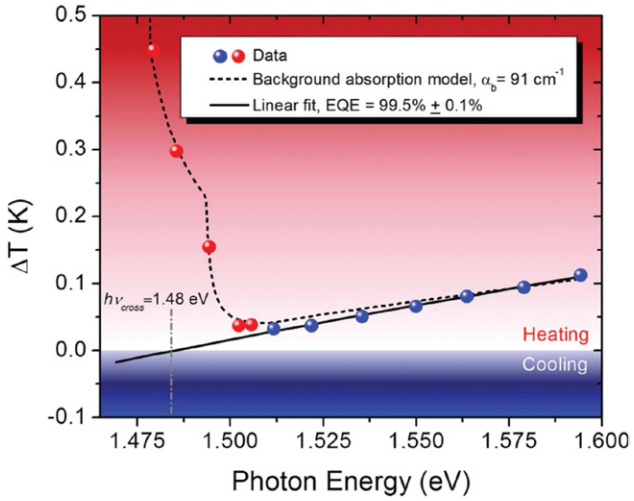

Figure 14. All-optical scanning laser calorimetry data for GaAs/GaInP DHS performed at 100 K. Each data point is the average of three measurements. Error bars are smaller than the size of the data points. The linear fit (equation (24)) gives an EQE of 99.5% (solid line) assuming $\eta_{abs} \sim 1$. Long wavelength data (red spheres) is used in fitting the background absorption model using equation (24) (dashed line).

for thicker layers with dominant surface recombination for thinner layers [110, 147, 148]. Most recently, Bender *et al* reported a record EQE ~99.5% in GaAs/GaInP DHS structure that was developed by a highly controlled MOCVD growth procedure at Sandia National Laboratories [93]. As shown in figure 14, despite such a high EQE value, the presence of parasitic absorption in the band-tail prevented the observation of net cooling at longer wavelengths.

While the laser cooling attempts in GaAs was being hindered by the large background absorption (whose origin is yet to be understood), researchers from Nanyang Technological University in Singapore reported observation of net cooling in CdS nanobelts at $\lambda \sim 520$ nm [92]. The samples, having a thickness of ~200 nm and an area ~10's μm^2, were synthesized by vapor-transport chemical vapor-deposition

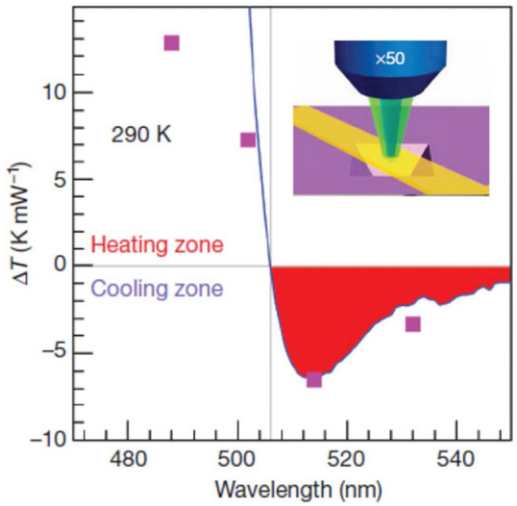

Figure 15. Fractional heating in CdS nanobelts in the vicinity of mean luminescence wavelength (indicated by thin vertical line at ~506 nm). Negative ΔT values, occurring for pump wavelengths above the mean luminescence wavelength correspond to cooling of the nanobelt (with permission from [92]). Copyright 2013 Nature Publishing Group.

system [136, 151]. Their data (employing TG-DLT method described earlier), is reproduced in figure 15. These results were a pleasant surprise as II–VI compounds were not known to exhibit the necessary EQE for optical refrigeration although they were expected to have extremely high purity and thus low parasitic absorption [152]. In retrospect, one may argue that lower carrier mobility (which is typical of these II–VI materials) favors the cooling condition as it leads to a slower surface recombination velocity, and subsequently smaller A-coefficient as it appears in equation (22). Additionally, the small Auger recombination rate C and a larger B coefficient (due to large band-gap of CdS) offers possible explanation for this observation. In short, these results have opened up a new frontier in the investigation of laser cooling of semiconductors. A better understanding of the CdS results, and potentially extending of these experiments to other II–VI compounds [153], will pave the way towards exploiting these materials for practical cryocooler devices. This quest however requires that cooling procedure can be scaled up to larger volumes suitable for assembly with a thermal link and integration with an actual load. Finally, it should be noted that phonon-assisted upconversion processes were also experimentally studied in GaN, another wide-gap semiconductor [154].

4. Device concepts

4.1. Device implementation

Laboratory studies have clearly shown the potential for using optical refrigeration for cooling loads to cryogenic temperatures. While there are no fundamental physics or thermodynamics barriers to harnessing the cryocooling capacity of optical refrigeration to cool a load, there are some interesting engineering challenges. These challenges mainly focus around thermally coupling the cooling element to the cold load

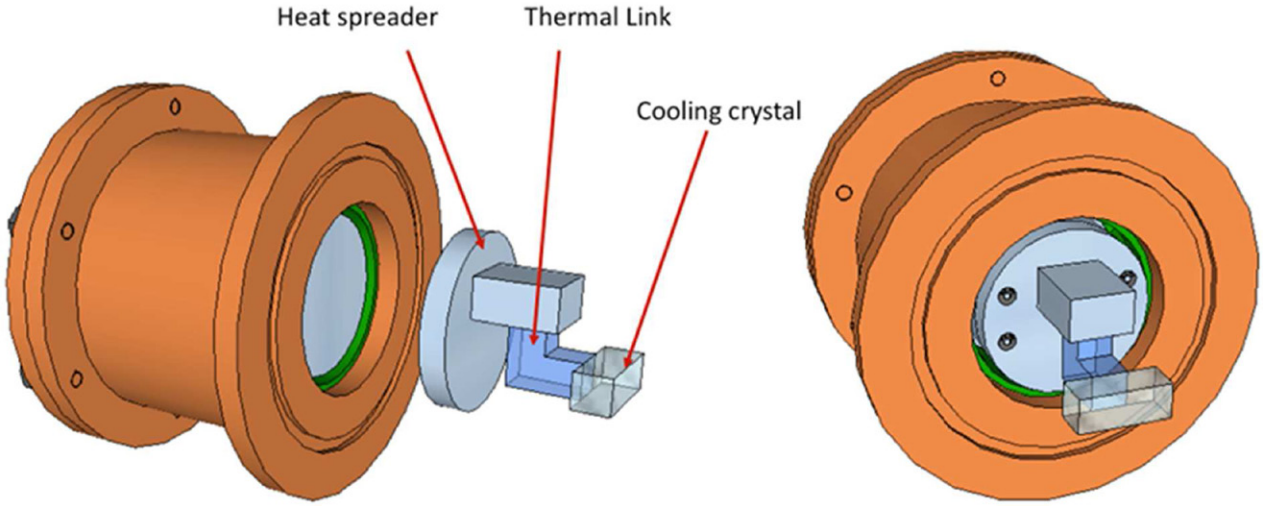

Figure 16. Cold components of a basic optical refrigerator. The cooling crystal loses heat by anti-Stokes fluorescence. Heat is conducted from the load through the heat spreader and thermal link to the cooling crystal. The thermal link is designed to minimize heat from fluorescent radiation reaching the heat spreader and cold load.

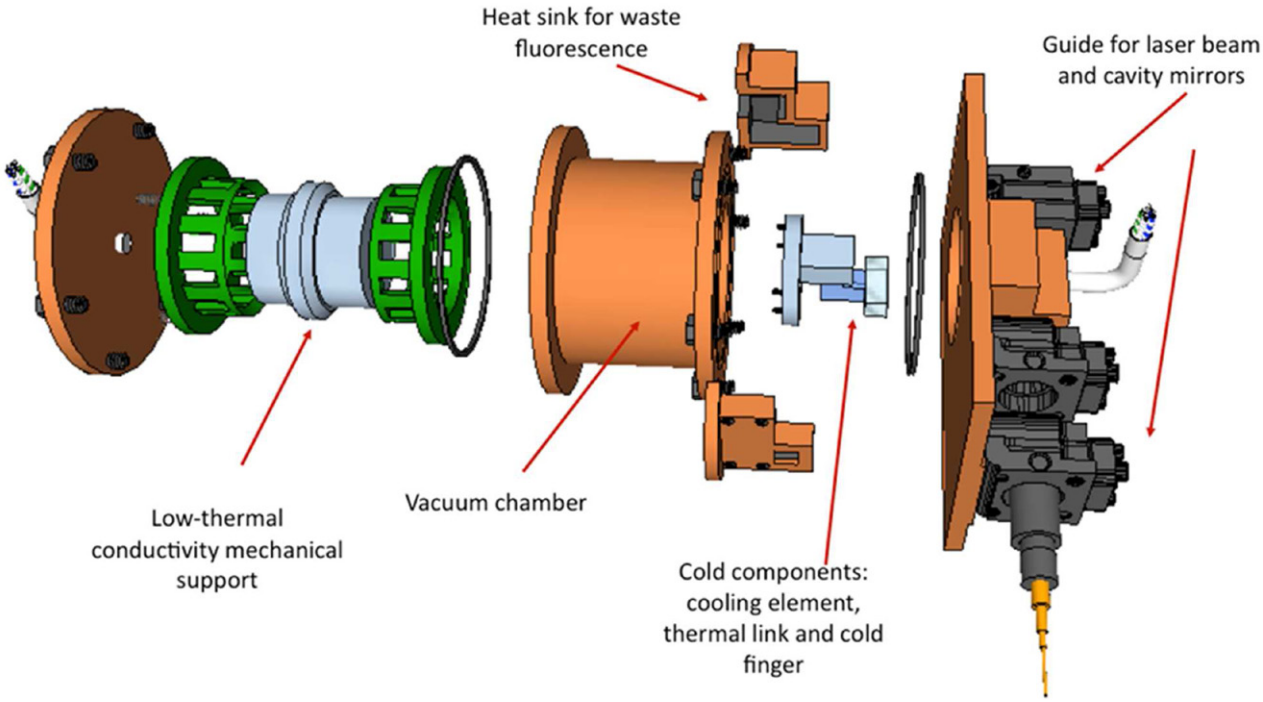

Figure 17. Exploded view of a basic optical refrigerator. The full optical refrigerator has components for delivering the laser power to the cooling element, removing the energy of the fluorescence, thermally isolating and mechanically supporting the cold components and maintaining a high vacuum.

while preventing the vast amount of fluorescent emission from generating unwanted heating. Since the power of the waste fluorescence is typically 50 times greater than the cooling heat lift, this coupling requires some care. As a rough analogy, it is as though one wants to use a 10 W refrigerator that had a 500 W refrigerator light bulb that can't be turned off.

Figures 16 and 17 illustrate the general approach to building and optical refrigerator that is being pursued by ThermoDynamic Films, LLC (TDF) and the University of New Mexico (UNM). The heart of the optical refrigerator is the cooling element, which removes heat when pumped with the appropriate laser light. The refrigerator has to connect the cooling element to the load in a way that minimizes heating of the load by the waste fluorescence or by heat leakage from the warm environment.

The cooling element is attached to a thermal link, which has a high thermal conductivity and very low absorptivity for both the fluorescence and the pump light. Currently, the TDF/UNM team is using sapphire thermal links. The thermal link is given a sharply kinked shape so that fluorescence or scattered pump light that enters the thermal link will exit it at the bend and not reach the 'heat spreader', which is connected to the load.

A functional optical refrigerator needs a number of other components. It has to have optics for delivering the laser

Table 1. Relative advantages of low-temperature cooling systems.

Feature \ Technology	Optical refrigerator	Thermoelectric coolers	Mechanical coolers
Solid state	Yes	Yes	No
Vibrations	None	None	Moderate
Reliability	High	High	Moderate
Cool below 180 K	Yes	No	Yes
Efficiency	Ok	No	Good
Cool below 60 K	No	No	Yes

beam to the device and a cavity for trapping the light until it is absorbed by the cooling element. The right side of figure 17 shows an adjustable, non-resonant pump and cavity scheme. The optical cavity is formed by two mirrors that are outside the vacuum chamber that contains the cooling crystal and all the cold components. The pump laser light enters the cavity through a small hole in one of the cavity mirrors. The light then passes through the cooling element, is reflected by the second mirror and returns through the cooling element. The light is repeatedly reflected between the two mirrors until it is largely absorbed in the cooing element. The cold components of the optical refrigerator, which includes the cooling element, the thermal link, heat spreader and load, are aligned so that the cooling element is held in the correct place in the optical cavity.

In the 'dark region' of the optical refrigerator, beyond the heat sink where the fluorescence is blocked, conventional cryoengineering techniques are used to support the cold elements. The left side of figure 17 shows a machined aerogel support structure to hold the cold elements in place. The support structure has to be optimized to provide rigid alignment while limiting the heat leakage from the environment. Another critical component of the refrigerator is the heat sink for the waste heat, which is shown near the middle of figure 17. The heat sink surrounds the cooling element and thermal link and absorbs the fluorescence and scattered pump light shed by these parts. The heat from this light is conducted to a distant thermal bath. Additionally, to lower the radiative heat leakage, the surfaces of the heat sink are coated to minimize the thermal emissivity [155].

4.2. Uses for optical refrigerators

Optical refrigerators bring a set of valuable capabilities to cryogenic cooling that are not met by traditional approaches such as mechanical refrigerators or cryogens [156].

The most distinctive advantages of optical refrigerators are their complete lack of vibrations, high reliability, and compactness. In some applications it may be useful that optical refrigerators do not generate electromagnetic interference (nor are they affected by it), and that they can be used in the presence of strong magnetic fields.

The main alternatives to optical refrigerators are mechanical coolers, such as Stirling cycle or pulsed tube technology, and thermoelectric cooler, which based on the Peltier effect. As the table 1 shows, each of these technologies has application areas where it most advantageous. For applications that require reliable, vibration-free cooling in the temperature range between 180 K and 60 K, optical refrigerators are the best solution (the lowest end of this temperature range, 60 K, is a credible goal that has not yet been demonstrated). The special properties of optical refrigerators make them well suited for a number of important applications, which are summarized in table 2.

Table 2. Applications that can benefit from optical refrigeration.

Applications	Advantages of optical refrigerators	Required temperature
Speed based Infrared cameras	No vibrations, high reliability, low mass	<150 K
Terrestrial Infrared cameras	High reliability	<150 K
Germanium gamma-ray spectrometers	No Vibrations	<110 K
Ultra-stable laser cavities	No Vibrations	124 K
Electron cryo-microscopy	No Vibrations	<170
Low noise amplifies	Low mass, high reliability	<170 K

The first applications listed are infrared (IR) cameras. These cameras are used for a broad range of military, surveillance, security and commercial applications. Because of their ability to image thermal IR light, these cameras are useful for night vision, tracking, search and rescue, nondestructive evaluation, gas analysis and condition monitoring. Cooled IR cameras, which use photon detectors, are many times more sensitive than uncooled cameras that employ microbolometers. The cooled cameras are therefore needed for taking fast or high-resolution images. In recent years, the development of high operating temperature detectors, *HOT* detectors, has made it possible to use high-performance imagers at temperatures as high as 150 K. This temperature is well within the operating range of optical refrigerators, but still far below what is achievable with Peltier devices; see, e.g. [157, 158]. Satellite-borne systems demand both low mass cooler and high reliability. The cost of the satellite missions increases dramatically with weight and repairs are usually impossible. Additionally, a vibration-free cooling system is very desirable for space-based imagers, since even slight motions of the cameras can severely degrade the image. In many terrestrial systems, the high reliability of solid-state optical refrigerators is attractive. It can be inconvenient or even dangerous if IR cameras used for surveillance or monitoring suffer too much down time because of cooler malfunctions.

Gamma-ray spectrometers with high-energy resolution and high-detection efficiency are needed to detect and identify nuclear materials. This capability is critical for homeland security applications and for the interdiction of smuggled nuclear material. Cooled high-purity germanium (HPGe) gamma-ray spectrometers are the best devices for these applications. These HPGe spectrometers need to be cooled to at least 120 K to perform well. Additionally, the cooling system must not produce significant vibrations. In HPGe spectrometers, a high-voltage circuit measures currents that give the number

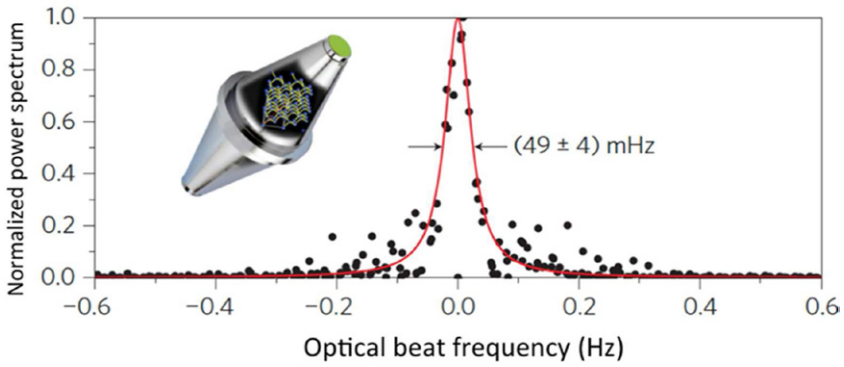

Figure 18. Optical heterodyne beat between the silicon cavity system and a reference laser. The data are the fourier transform of the beat signal and the red line is a Lorentzian fit that highlights the laser's extreme stability. The insert is a drawing of the single-crystal cavity (with permission from [160]). Copyright Nature Publishing Group.

of electron–hole pairs generated by the incoming gamma rays. Even minor motions generate variable capacitance that generates noise in the currents and blurs the gamma-ray spectra [159]. Vibration-free optical refrigeration can provide a clear advantage for these devices.

Ultrastable lasers and interferometers are critical for the most accurate measuring science. This science includes gravitational wave detection, cavity quantum electrodynamics, quantum optomechanics and precision tests of relativity. On a more commercial level, the ability to measure and precisely control laser frequencies promises tremendous advances in the performance of atomic clocks and frequency standards which will define the next generation of navigation and communication standards.

The sensitivity and stability of the lasers is ultimately set by Brownian noise in the spaces and mirrors of the laser cavity. Researches at NIST [160] greatly reduced this noise by creating a laser interferometric cavity from single-crystal silicon. Cooling the cavity to 124 K, where the coefficient of thermal expansion of silicon is zero, makes it insensitive to temperature fluctuations. With this optical cavity, they were able to demonstrate the most stable oscillator of any kind; see figure 18. The cooling system for these cavities has to be essentially vibration-free. Currently the cavity is cooled with nitrogen vapor. Optical refrigerator is only cooling technology on the horizon that can be used to make this type of laser cavity portable and rugged.

Electron cryo-microscopy and the related cryo-electron tomography allow investigators to determine the structure of biological macromolecules in the cell. These structures are measured at near-atomic resolution (a few angstroms) by averaging thousands of electron microscope images of cryocooled samples, which are recorded before radiation damage accumulates. This capability gives molecular biology new tools to study structures at near-atomic resolution that complements those of x-ray crystallography and nuclear magnetic resonance spectroscopy [161]. The samples in electron cryo-microscopes are generally cooled by liquid nitrogen, with the attendant complexities and size associated with dewars and flow controls. Mechanical coolers could not be used because their vibrations, and thermoelectric coolers do not go to low enough temperatures. Vibration-free optical refrigerators could be used instead of liquid nitrogen to reduce the complexity and increase the stability of electron cryo-microscopes.

The low mass, compactness and high reliability of optical refrigerators can make them very useful for cooling low noise amplifiers (LNA) in antenna systems. The sensitivity of antenna systems depends on the noise figure of the LNA and improves when LNA is cooled. By cooling the LNA, an antenna system can achieve the same sensitivity with smaller active area. This reduction in the size and mass of an antenna can be especially important in fast-tracking systems, which require antennas to slew rapidly. Recent experiments have shown that cooling the LNA to 115 K can allow the antenna area to be reduced by about 43% [162].

5. Outlook: challenges and prospects

The next few years should see optical refrigerators deployed to cool electronic and optical devices. The initial specialized applications will be driven by their unique characteristic of being the only vibration-free coolers at cryogenic temperatures. Additional applications will become viable as the efficiency of the optical refrigerators improves and their mass and cost decrease. These developments require overcoming a number of engineering and scientific challenges in developing the refrigerators and adapting the electronic and optical devices to take advantage of this new cooing architecture.

The initial optical refrigerators require all of the components of the device be brought together in a compact, rugged unit such as shown in figure 17. This device employs an optical cavity and laser driver similar to what is currently used in laboratory, bench top experiments. In particular, it uses a single-mode fiber laser with a two-mirror non-resonant laser cavity to pump to an ytterbium-doped YLF cooling crystal. The cold crystal is connected to the cold finger by a sapphire thermal link. This type of device is well suited to applications where the main driver is removing all vibrations from the cooler and cost, efficiency, weight and size are secondary. These applications include cooling the ultrastable laser cavity for advance metrology and electron cryo-microscopy.

Later generations of optical refrigerators, which will be more efficient, compact and cost effective, will be suitable for the larger markets of infrared cameras and gamma ray

spectrometers. Employing efficient, multimode diode laser rather than a single mode fiber laser can significantly reduce the cost and power requirements of the optical refrigerators. However, the lower beam quality of the diode laser requires that the refrigerator use a more accepting optical cavity for pumping the cooling crystal. One possibility is using a mirrored cooling crystal as described in Edwards *et al* [97]. This cavity traps the pump light with low-loss mirrors deposited on the ends of the cooling crystal and relies on total internal reflection to avoid losing light through the side surfaces. The light enters the cooling crystal through a pinhole in one of the mirrors and can only escape by exiting through the same hole. Fixing a small ratio of the pinhole size to that of the mirror, gives a high pumping efficiency even for unpolarized pump beam with moderately high numerical aperture.

Recycling the waste fluorescence further increases the efficiency of the optical refrigerators. One approach is to capture the fluorescence with photovoltaic cells and funnel the resulting electrical power into the driver for the laser. With existing photovoltaic cells and diode lasers, a factor of two increase in efficiency is reasonable. This approach has the additional advantage that converting the fluorescent light to electrical power also decreases the amount of heat that has to be removed from the walls of the chamber that houses the cooling crystal. A second recycling scheme does not require photovoltaic cells. Instead absorbing material in the chamber with the cooling crystal absorbs waste fluorescence and reemits it at longer wavelengths (Stokes shift) where it can again be used to drive the cooling process.

While advancing the optical refrigeration towards practical application, as described above, is taking shape the quest for reaching lower and lower temperatures fuels further fundamental investigations in this field. In the area of rare-earth doped systems, significant reduction in the minimum achievable temperature is intimately tied to drastic advances in material growth. In particular, as simple analysis in section 2 leading to equation (5) suggested, developing host materials with narrower ground-state manifold play the key role in keeping the absorption efficiency high at temperatures approaching 50 K and possibly lower. Interestingly, we note that this requirement is totally opposite of what a suitable laser host demands which is a wider ($\gg k_B T$) manifold. Undertaking such endeavor involves deeper understanding followed by utilization of the crystal-field (Stark) engineering in potential host [60, 163]. In parallel, continuing efforts in developing extremely high purity crystals with a parasitic absorption approaching less than 10^{-5} cm^{-1} while maintaining (or increasing) the doping concentration of the RE-ion to $>10\%$ without degradation of quantum efficiency will play an essential role in realizing the 50 K milestone. Identification of the iron impurities in Yb:YLF crystals [62] presented a major step towards that direction. It remains to be seen if lowering such transition metal impurities and increasing the doping concentration can simultaneously be attained in cooling grade crystals. In addition to Yb-doped crystals which have thus far produced the only cryogenic operation, ions with lower ground-state transitions such as erbium, thulium, holmium and dysprosium have been touted as pathways to enhancing the cooling efficiency by virtue of the energy-gap scaling of equation (1). Cooling in erbium and thulium doped systems has already been reported and in particular this scaling law has been shown to hold for thulium-doped systems [50, 52]. Recently proposed co-doping strategies should also be analyzed further [119]. With advances in the development of efficient and high-power mid-IR lasers, exploiting low-gap RE-doped crystals for high-efficiency cryo-cooling applications are increasingly more appealing. The material synthesis challenges however remain with even more stringent requirement on low-phonon energy hosts in order to render nonradioactive decay rates insignificant. This requirement may be particularly arduous for Dy-doped systems having a ground-state transition of ~0.4 eV ($\lambda \sim 3\ \mu$m), but the three-fold gain in efficiency over Yb-doped coolers makes this system a promising and worthy area of investigation.

Speaking of high risks and high rewards, direct laser cooling of semiconductors rightfully receives considerable attention for their potential in achieving far lower temperatures than their rare-earth counterparts, as described in section 3. The recent demonstration of net cooling in CdS structures has opened up a new frontier in this field. A better understating of the underlying mechanism that has resulted in such high quantum efficiencies reported in such un-passivated nanostructures [91] should pave the way for scaling-up these systems to larger sizes, lower temperatures and higher heat loads. More importantly, it should provide clear pathways to potential cooling of other II-VI compounds with lower band-gaps such as CdSe and CdTe. Finally, with further and deeper investigation into the GaAs heterostructures, it is anticipated that we soon understand the origin of the observed bandtail parasitic absorption, and thus mitigate it to achieve net cooling. A successful demonstration of net laser cooling in GaAs or any III–V compounds will mark another major milestone in the field of solid-state laser cooling.

Acknowledgments

ThermoDynamic Films and the University of New Mexico received support for this work from the AFRL under SBIR contracts FA9453-14-M-0055 and FA9453-14-C-0304 and from the AFOSR under STTR contract FA9550-13-C-0006. DVS acknowledges partial support from the National Science Foundation (Grant No. 1160764), the EU FP7 Marie Curie Zukunftskolleg Incoming Fellowship Programme at University of Konstanz (Grant No. 291784) and the Baden–Württemberg–Stiftung through the 'Eliteprogramm für Postdoktorandinnen und Postdoktoranden'. The authors also acknowledge Seth Melgaard, Alexander Albrecht, Chengao Wang, Mohammad Ghasemkhani for their experimental contributions, and Markus Hehlen for useful discussions.

References

[1] Hansch T W and Schawlow A L 1975 Cooling of gases by laser radiation *Opt. Commun.* **13** 68–9
[2] Chu S 1998 Nobel lecture: the manipulation of neutral particles *Rev. Mod. Phys.* **70** 685–706

[3] Jin D S and Ye J 2011 Polar molecules in the quantum regime *Phys. Today* **64** 27

[4] Chu S, Hollberg L, Bjorkholm J E, Cable A and Ashkin A 1985 3D viscous confinement and cooling of atoms by resonance radiation pressure *Phys. Rev. Lett.* **55** 48–51

[5] Cornell E A and Wieman C E 2002 Nobel lecture: Bose–Einstein condensation in a dilute gas, the first 70 years and some recent experiments *Rev. Mod. Phys.* **74** 875–93

[6] Berman P R and Stenholm S 1978 Heating or cooling collisionally aided fluorescence *Opt. Commun.* **24** 155–7

[7] Vogl U and Weitz M 2009 Laser cooling by collisional redistribution of radiation *Nature* **461** 70–4

[8] Epstein R I, Buchwald M I, Edwards B C, Gosnell T R and Mungan C E 1995 Observation of laser-induced fluorescent cooling of a solid *Nature* **377** 500–3

[9] Djeu N and Whitney W T 1981 Laser cooling by spontaneous anti-stokes scattering *Phys. Rev. Lett.* **46** 236–9

[10] Clark J L and Rumbles G 1996 Laser cooling in the condensed phase by frequency up-conversion *Phys. Rev. Lett.* **76** 2037–40

[11] Melgaard S D, Seletskiy D V, Albrecht A R and Sheik-Bahae M 2015 First solid-state cooling below 100 K *SPIE Newsroom* online

[12] Melgaard S D, Albrecht A R, Hehlen M P and Sheik-Bahae M 2016 Solid-state optical refrigeration to sub-100 Kelvin regime *Sci. Rep.* **6** 20380

[13] Rogalski A 2010 *Infrared Detectors* 2nd edn (Boca Raton, FL: CRC Press)

[14] Knoll G F 2000 *Radiation Detection and Measurement* (New York: Wiley)

[15] Zhou C, Birner S, Tang Y, Heinselman K and Grayson M 2013 Driving perpendicular heat flow: $(p \times n)$-type transverse thermoelectrics for microscale and cryogenic peltier cooling *Phys. Rev. Lett.* **110** 227701

[16] Mills G and Mord A 2005 Performance modeling of optical refrigerators *Cryogenics* **46** 176–82

[17] Stokes G G 1852 On the change of refrangibility of light *Phil. Trans. R. Soc.* **142** 463–562

[18] Pringsheim P 1929 Zwei bemerkungen uber den unterschied von lumineszenz- und temperaturstrahlung *Z. Phys.* **57** 739–46

[19] Vavilov S I 1946 Photoluminescence and thermodynamics *J. Phys. USSR* **10** 499–501

[20] Landau L 1946 On the thermodynamics of photoluminescence *J. Phys. Mosc.* **10** 503–6

[21] Lloyd S 1997 Quantum-mechanical Maxwell's demon *Phys. Rev.* A **56** 3374–82

[22] Scovil H E D and Schulz-DuBois E O 1959 Three-level masers as heat engines *Phys. Rev. Lett.* **2** 262–3

[23] Seletskiy D V, Hehlen M P, Epstein R I and Sheik-Bahae M 2012 Cryogenic optical refrigeration *Adv. Opt. Photonics* **4** 78–107

[24] Kastler A 1950 Some suggestions concerning the production and detection by optical means of inequalities in the populations of levels of spatial quantization in atoms. Application to the Stern and Gerlach and magnetic resonance experiments *J. Phys. Radium* **11** 11

[25] Yatsiv S 1961 *Anti-Stokes fluorescence as a Cooling Process* ed J R Singer (New York: Columbia University)

[26] Sheik-Bahae M and Epstein R I 2009 Laser cooling of solids *Laser Photon. Rev.* **3** 67–84

[27] Kushida T and Geusic J E 1968 Optical refrigeration in Nd-doped yttrium aluminum garnet *Phys. Rev. Lett.* **21** 1172–5

[28] Agrawal G 2012 *Nonlinear Fiber Optics* 5th edn (Amsterdam: Academic)

[29] Mungan C E, Buchwald M I, Edwards B C, Epstein R I and Gosnell T R 1997 Laser cooling of a solid by 16 K starting from room temperature *Phys. Rev. Lett.* **78** 1030

[30] Luo X, Eisaman M D and Gosnell T R 1998 Laser cooling of a solid by 21K starting from room temperature *Opt. Lett.* **23** 639–41

[31] Thiede J, Distel J, Greenfield S R and Epstein R I 2005 Cooling to 208 K by optical refrigeration *Appl. Phys. Lett.* **86** 154107

[32] Edwards B C, Anderson J E, Epstein R I, Mills G L and Mord A J 1999 Demonstration of a solid-state optical cooler: an approach to cryogenic refrigeration *J. Appl. Phys.* **86** 6489

[33] Rayner A, Friese M E J, Truscott A G, Heckenberg N R and Rubinsztein-dunlop H 2001 Laser cooling of a solid from ambient temperature *J. Mod. Opt.* **48** 103–14

[34] Murtagh M T, Sigel G H Jr, Fajardo J C, Edwards B C and Epstein R I 1999 Laser-induced fluorescent cooling of rare-earth-doped fluoride glasses *J. Non-Cryst. Solids* **253** 50–7

[35] Rayner A, Heckenberg N R and Rubinsztein-Dunlop H 2003 Condensed-phase optical refrigeration *J. Opt. Soc. Am.* B **20** 1037–53

[36] Heeg B, Stone M D, Khizhnyak A, Rumbles G, Mills G and DeBarber P A 2004 Experimental demonstration of intracavity solid-state laser cooling of Yb^{3+}:$ZrF_4-BaF_2-LaF_3-AlF_3-NaF$ glass *Phys. Rev.* A **70** 021401

[37] Patterson W M, Seletskiy D V, Sheik-Bahae M, Epstein R I and Hehlen M P 2010 Measurement of solid-state optical refrigeration by two-band differential luminescence thermometry *J. Opt. Soc. Am.* B **27** 611–8

[38] Mungan C E and Gosnell T R 1999 *Laser Cooling of Solids* vol 40 (New York: Academic) pp 161–228

[39] Fernández J, Mendioroz A, García A J, Balda R, Adam J L and Arriandiaga M A 2001 On the origin of anti-Stokes laser-induced cooling of Yb^{3+}-doped glass *Opt. Mater.* **16** 173–9

[40] Fernández J, Mendioroz A, García A J, Balda R and Adam J L 2000 Anti-Stokes laser-induced internal cooling of Yb^{3+}-doped glasses *Phys. Rev.* B **62** 3213–7

[41] Bowman S R and Mungan C E 2000 New materials for optical cooling *Appl. Phys.* B **71** 807–11

[42] Epstein R I, Brown J J, Edwards B C and Gibbs A 2001 Measurements of optical refrigeration in ytterbium-doped crystals *J. Appl. Phys.* **90** 4815

[43] Filho E S de L, Nemova G, Loranger S and Kashyap R 2013 Laser-induced cooling of a Yb:YAG crystal in air at atmospheric pressure *Opt. Express* **21** 24711–20

[44] Bigotta S 2006 Spectroscopic and laser cooling results on Yb^{3+}-doped BaY2F8 single crystal *J. Appl. Phys.* **100** 013109

[45] Bigotta S, Parisi D, Bonelli L, Toncelli A, Lieto A D and Tonelli M 2006 Laser cooling of Yb^{3+}-doped BaY2F8 single crystal *Opt. Mater.* **28** 1321–4

[46] Bigotta S 2007 Laser cooling of solids: new results with single fluoride crystals *Nuovo Cimento B Ser.* **122** 685694

[47] Bigotta S, Di Lieto A, Parisi D, Toncelli A and Tonelli M 2007 Single fluoride crystals as materials for laser cooling applications *SPIE* **6461** 64610E

[48] Seletskiy D V, Melgaard S D, Bigotta S, Di Lieto A, Tonelli M and Sheik-Bahae M 2010 Laser cooling of solids to cryogenic temperatures *Nat. Photon.* **4** 161–4

[49] Guiheen J V, Haines C D, Sigel G H, Epstein R I, Thiede J and Patterson W M 2006 Yb^{3+} and Tm^{3+}-doped fluoroaluminate classes for anti-Stokes cooling *Phys. Chem. Glasses* **47** 167–76

[50] Hoyt C W, Sheik-Bahae M, Epstein R I, Edwards B C and Anderson J E 2000 Observation of anti-stokes fluorescence cooling in thulium-doped glass *Phys. Rev. Lett.* **85** 3600

[51] Hoyt C W, Hasselbeck M P, Sheik-Bahae M, Epstein R I, Greenfield S, Thiede J, Distel J and Valencia J 2003 Advances in laser cooling of thulium-doped glass *J. Opt. Soc. Am.* B **20** 1066–74

[52] Patterson W, Bigotta S, Sheik-Bahae M, Parisi D, Tonelli M and Epstein R 2008 Anti-Stokes luminescence cooling of Tm^{3+}doped BaY2F8 *Opt. Express* **16** 1704–10

[53] Rostami S, Albercht A R, Ghasemkhani M R, Melgaard S D, Gragossian A, Tonelli M and Sheik-Bahae M 2016 Optical refrigeration of Tm:YLF and Ho:YLF crystals *Proc. SPIE* **9765** 97650P

[54] Fernandez J, Garcia-Adeva A J and Balda R 2006 Anti-stokes laser cooling in bulk erbium-doped materials *Phys. Rev. Lett.* **97** 033001

[55] Condon N J, Bowman S R, O'Connor S P, Quimby R S and Mungan C E 2009 Optical cooling in Er^{3+}:KPb2Cl5 *Opt. Express* **17** 5466–72

[56] Sheik-Bahae M and Epstein R I 2007 Optical refrigeration *Nat. Photon.* **1** 693–9

[57] Epstein R and Sheik-Bahae M 2009 *Optical Refrigeration: Science and Applications of Laser Cooling of Solids* (New York: Wiley)

[58] Petrushkin S V and Samartsev V V 2009 *Laser Cooling of Solids* (Cambridge: Cambridge International Science Publishing)

[59] Nemova G and Kashyap R 2010 Laser cooling of solids *Rep. Prog. Phys.* **73** 086501

[60] Hehlen M P, Sheik-Bahae M, Epstein R I, Melgaard S D and Seletskiy D V 2013 Materials for optical cryocoolers *J. Mater. Chem.* C **1** 7471–8

[61] Melgaard S D, Seletskiy D V, Di Lieto A, Tonelli M and Sheik-Bahae M 2013 Optical refrigeration to 119 K, below National institute of standards and technology cryogenic temperature *Opt. Lett.* **38** 1588–90

[62] Melgaard S, Seletskiy D, Polyak V, Asmerom Y and Sheik-Bahae M 2014 Identification of parasitic losses in Yb:YLF and prospects for optical refrigeration down to 80K *Opt. Express* **22** 7756

[63] Vermeulen N, Debaes C, Muys P and Thienpont H 2007 Mitigating heat dissipation in raman lasers using coherent anti-stokes Raman scattering *Phys. Rev. Lett.* **99** 093903

[64] Rand S C 2012 Laser cooling of solids by stimulated Raman scattering and fluorescence *Proc. SPIE* **8275** 8275–08

[65] Ivanov A V and Rozhdestvensky Y V 2015 Laser cooling of doped crystals by methods of coherent pumping *Proc. SPIE* **9380** 93800S0S

[66] Chen Y-C and Bahl G 2015 Raman cooling of solids through photonic density of states engineering *Optica* **2** 893

[67] Petrushkin S V and Samartsev V V 2001 Superradiance regime of laser cooling of crystals and glasses doped with rare-earth ion *Laser Phys.* **11** 948–56

[68] Nemova G and Kashyap R 2011 Alternative technique for laser cooling with superradiance *Phys. Rev.* A **83** 013404

[69] Babajanyan V G 2013 Spectroscopic study of the expected optical cooling effect of $LiNbO_3$:Er^{3+} crystal *Laser Phys.* **23** 126002

[70] Nemova G and Kashyap R 2012 Laser cooling with PbSe colloidal quantum dots *J. Opt. Soc. Am.* B **29** 676–82

[71] Nemova G and Kashyap R 2015 Optical refrigeration of Yb^{3+}:YAG nanocrystals *Proc. SPIE* **9380** 938008

[72] Roder P B, Smith B, Zhou X, Crane M J and Pauzauskie P J 2015 Laser-refrigeration of rare-earth-doped nanocrystals in water *Proc. SPIE* **9380** 938007

[73] Roder P B, Smith B E, Zhou X, Crane M J and Pauzauskie P J 2015 Laser refrigeration of hydrothermal nanocrystals in physiological media *Proc. Natl Acad. Sci.* **112** 15024–9

[74] Nemova G and Kashyap R 2012 Laser cooling with Tm^{3+}-doped oxy-fluoride glass ceramic *J. Opt. Soc. Am.* B **29** 3034

[75] Krishnaiah K V, Soares de Lima Filho E, Ledemi Y, Nemova G, Messaddeq Y and Kashyap R 2016 Development of ytterbium-doped oxyfluoride glasses for laser cooling applications *Sci. Rep.* **6** 21905

[76] Santhanam P, Gray D J and Ram R J 2012 Thermoelectrically pumped light-emitting diodes operating above unity efficiency *Phys. Rev. Lett.* **108** 097403

[77] Malyutenko V K, Bogatyrenko V V and Malyutenko O Y 2013 Radiative cooling by light down conversion of InGaN light emitting diode bonded to a Si wafer *Appl. Phys. Lett.* **102** 241102

[78] Bowman S R 1999 Lasers without internal heat generation *IEEE J. Quantum Electron.* **35** 115–22

[79] Andrianov S N and Samartsev V V 2001 Solid state lasers with internal laser refrigeration effect *SPIE* **4605** 208–13

[80] Nemova G and Kashyap R 2009 Raman fiber amplifier with integrated cooler *J. Lightwave Technol.* **27** 5597–601

[81] Nguyen D T, Shanor C, Zong J, Tian W, Yao Z, Wu J, Weiss J, Binder R and Chavez-Pirson A 2011 Conceptual study of a fiber-optical approach to solid-state laser cooling *Proc. SPIE* **7951** 795109

[82] Nguyen D T, Zong J, Rhonehouse D, Miller A, Yao Z, Hardesty G, Kwong N H, Binder R and Chavez-Pirson A 2012 All fiber approach to solid-state laser cooling *Proc. SPIE* **8275** 827506

[83] Nguyen D T, Thapa R, Rhonehouse D, Zong J, Miller A, Hardesty G, Kwong N H, Binder R and Chavez-Pirson A 2013 Towards all-fiber optical coolers using Tm-doped glass fibers *Proc. SPIE* **8638** 86380G

[84] Vahala K J 2003 Optical microcavities *Nature* **424** 839–46

[85] Kippenberg T J and Vahala K J 2007 Cavity opto-mechanics *Opt. Express* **15** 17172–205

[86] Bahl G, Tomes M, Marquardt F and Carmon T 2011 Observation of spontaneous brillouin cooling *Nat. Phys.* **8** 203–7

[87] Favero I, Sankey J, Weig E M, Sankey J and Favero I 2014 Mechanical resonators in the middle of an optical cavity *Cavity Optomechanics Quantum Science and Technology* ed M Aspelmeyer *et al* (Berlin: Springer) pp 83–119

[88] Teufel J D, Donner T, Li D, Harlow J W, Allman M S, Cicak K, Sirois A J, Whittaker J D, Lehnert K W and Simmonds R W 2011 Sideband cooling of micromechanical motion to the quantum ground state *Nature* **475** 359–63

[89] Aspelmeyer M, Kippenberg T J and Marquardt F 2014 Cavity optomechanics *Rev. Mod. Phys.* **86** 1391–452

[90] Hoyt C 2003 *Laser Cooling in Thulium-Doped Solids* (Albuquerque, NM: University of New Mexico)

[91] Zhang J, Li D H, Chen R J and Xiong Q H 2013 Laser cooling of a semiconductor by 40 Kelvin *Nature* **493** 504–8

[92] Ha S-T, Shen C, Zhang J and Xiong Q 2016 Laser cooling of organic–inorganic lead halide perovskites *Nat. Photon.* **10** 115–21

[93] Bender D A, Cederberg J G, Wang C and Sheik-Bahae M 2013 Development of high quantum efficiency GaAs/GaInP double heterostructures for laser cooling *Appl. Phys. Lett.* **102** 252102–5

[94] Emin D 2007 Laser cooling via excitation of localized electrons *Phys. Rev.* B **76** 024301

[95] Sheik-Bahae M and Epstein R I 2004 Can laser light cool semiconductors? *Phys. Rev. Lett.* **92** 247403

[96] Kohmoto T, Fukuda Y, Kunitomo M and Isoda K 2000 Observation of ultrafast spin-lattice relaxation in Tm^{2+}-doped CaF2 and SrF2 crystals by optical means *Phys. Rev.* B **62** 579–83

[97] Edwards B C, Buchwald M I and Epstein R I 1998 Development of the Los Alamos solid-state optical refrigerator *Rev. Sci. Instrum.* **69** 2050

[98] Mungan C E 2005 Radiation thermodynamics with applications to lasing and fluorescent cooling *Am. J. Phys.* **73** 315–22

[99] Ruan X L, Rand S C and Kaviany M 2007 Entropy and efficiency in laser cooling of solids *Phys. Rev.* B **75** 214304

[100] Edwards B C, Buchwald M I and Epstein R I 2000 Optical refrigerator using reflectivity tuned dielectric mirrors *US Patent* 6041610 A

[101] Frey R, Micheron F and Pocholle J P 2000 Comparison of peltier and anti-Stokes optical coolings *J. Appl. Phys.* **87** 4489–98

[102] Sheik-Bahae M 2015 *Provisional Patent* University of New Mexico, STC Ref. 2015-047

[103] Seletskiy D V, Melgaard S D, Epstein R I, Di Lieto A, Tonelli M and Sheik-Bahae M Precise determination of minimum achievable temperature for solid-state optical refrigeration *J. Lumin.*

[104] McCumber D E 1964 Einstein relations connecting broadband emission and absorption spectra *Phys. Rev.* **136** A954–7

[105] Seletskiy D V, Melgaard S D, Epstein R I, Di Lieto A, Tonelli M and Sheik-Bahae M 2011 Local laser cooling of Yb:YLF to 110 K *Opt. Express* **19** 18229–36

[106] Sugiyama A, Katsurayama M, Anzai Y and Tsuboi T 2006 Spectroscopic properties of Yb doped YLF grown by a vertical Bridgman method *J. Alloys Compd.* **408-12** 780–3

[107] Filho E S de L, Baiad M D, Gagné M and Kashyap R 2014 Fiber Bragg gratings for low-temperature measurement *Opt. Express* **22** 27681–94

[108] Seletskiy D V, Hasselbeck M P, Sheik-Bahae M and Epstein R I 2009 Fast differential luminescence thermometry *Proc. SPIE Laser Refrigeration of Solids II (San Jose, CA)* p 72280K

[109] Imangholi B, Hasselbeck M P, Bender D A, Wang C, Sheik-Bahae M, Epstein R I and Kurtz S 2006 Differential luminescence thermometry in semiconductor laser cooling *Proc SPIE* **6115** 61151C

[110] Wang C, Li C-Y, Hasselbeck M P, Imangholi B and Sheik-Bahae M 2011 Precision, all-optical measurement of external quantum efficiency in semiconductors *J. Appl. Phys.* **109** 093108

[111] Melgaard S D 2013 Cryogenic optical refrigeration: laser cooling of solids below 123 K

[112] Herriott D R and Schulte H J 1965 Folded optical delay lines *Appl. Opt.* **4** 883–9

[113] Siegman A E 1986 *Lasers* (Mill Valley, CA: University Science Books)

[114] Seletskiy D V, Hasselbeck M P and Sheik-Bahae M 2010 Resonant cavity-enhanced absorption for optical refrigeration *Appl. Phys. Lett.* **96** 181106

[115] Heeg B, Rumbles G, Khizhnyak A and DeBarber P A 2002 Comparative intra- versus extra-cavity laser cooling efficiencies *J. Appl. Phys.* **91** 3356–62

[116] Ghasemkhani M, Albrecht A R, Melgaard S D, Seletskiy D V, Cederberg J G and Sheik-Bahae M 2014 Intra-cavity cryogenic optical refrigeration using high power vertical external-cavity surface-emitting lasers (VECSELs) *Opt. Express* **22** 16232

[117] Hehlen M P, Epstein R I and Inoue H 2007 Model of laser cooling in the Yb^{3+}-doped fluorozirconate glass ZBLAN *Phys. Rev.* B **75** 144302

[118] Di Lieto A, Sottile A, Volpi A, Zhang Z, Seletskiy D V and Tonelli M 2014 Influence of other rare earth ions on the optical refrigeration efficiency in Yb:YLF crystals *Opt. Express* **22** 28572

[119] Volpi A, Di Lieto A and Tonelli M 2015 Novel approach for solid state cryocoolers *Opt. Express* **23** 8216–26

[120] Oraevsky A N 1996 Cooling of semiconductors by laser radiation *J Russ. Laser Res.* **17** 471–9

[121] Zadernovskii A A and Rivlin L A 1996 Laser cooling of a semiconductor (optical heat engine) *Kvantovaya Elektron.* **23** 1131–3

[122] Gauck H, Gfroerer T H, Renn M J, Cornell E A and Bertness K A 1997 External radiative quantum efficiency of 96% from a GaAs/GaInP heterostructure *Appl. Phys. Mater. Sci. Process.* **64** 143–7

[123] Rivlin L A and Zadernovsky A A 1997 Laser cooling of semiconductors *Opt. Commun.* **139** 219–22

[124] Gfroerer T H, Cornell E A and Wanlass M W 1998 Efficient directional spontaneous emission from an InGaAs/InP heterostructure with an integral parabolic reflector *J. Appl. Phys.* **84** 5360–2

[125] Finkeissen E, Potemski M, Wyder P, Vina L and Weimann G 1999 Cooling of a semiconductor by luminescence up-conversion *Appl. Phys. Lett.* **75** 1258–60

[126] Sheik-Bahae M, Hasselbeck M P and Epstein R I 2002 Prospects for Laser Cooling in Semiconductors *Quantum Electron. Laser Sci. (QELS'02 Technical Digest)* 103

[127] Rupper G, Kwong N H and Binder R 2006 Theory of semiconductor laser cooling at low temperatures *Phys. Status Solidi c* **3** 2489–93

[128] Khurgin J B 2006 Band gap engineering for laser cooling of semiconductors *J. Appl. Phys.* **100** 113116

[129] Khurgin J B 2006 Band gap engineering for laser cooling of semiconductors *SPIE* **6115** 611519

[130] Khurgin J B 2007 Surface plasmon-assisted laser cooling of solids *Phys. Rev. Lett.* **98** 177401

[131] Khurgin J B 2008 Role of bandtail states in laser cooling of semiconductors *Phys. Rev.* B **77** 235206

[132] Li J 2007 Laser cooling of semiconductor quantum wells: Theoretical framework and strategy for deep optical refrigeration by luminescence upconversion *Phys. Rev.* B **75** 155315

[133] Rupper G, Kwong N H and Binder R 2006 Large excitonic enhancement of optical refrigeration in semiconductors *Phys. Rev. Lett.* **97** 117401

[134] Kwong N H, Rupper G, Gu B and Binder R 2007 The relation between light absorption and luminescence in laser cooling of 2D semiconductor *Laser Cooling Solids* **6461** I4610

[135] Wang J-B, Johnson S R, Ding D, Yu S-Q, Zhang Y-H, Yu S-Q, Ding D, Johnson S R and Wang J-B 2006 Influence of photon recycling on semiconductor luminescence refrigeration *J. Appl. Phys.* **100** 043502

[136] Li D, Zhang J and Xiong Q 2013 Laser cooling of CdS nanobelts: thickness matters *Opt. Express* **21** 19302–10

[137] Rupper G, Kwong N H and Binder R 2007 Optical refrigeration of GaAs: theoretical study *Phys. Rev.* B **76** 245203

[138] Rupper G, Kwong N H, Gu B and Binder R 2008 Theory of luminescence and optical refrigeration in p-doped semiconductors *Proc. SPIE* **6907** 690705

[139] Rupper G, Kwong N H, Binder R, Li C-Y and Sheik-Bahae M 2010 Effect of n-p-n heterostructures on interface recombination and semiconductor laser cooling *J. Appl. Phys.* **108** 113118

[140] Rupper G, Kwong N H and Binder R 2009 The role of finite spatial beam profiles on photo-luminescence and laser cooling in GaAs structures *Proc. SPIE* **7228** 722805

[141] Khurgin J B 2014 Multi-phonon-assisted absorption and emission in semiconductors and its potential for laser refrigeration *Appl. Phys. Lett.* **104** 221115

[142] Rupper G, Kwong N H, Gu B and Binder R 2008 Theory of laser cooling of semiconductor quantum wells *Phys. Status Solidi* b **245** 1049–54

[143] Basu P K 2003 *Theory of Optical Processes in Semiconductors: Bulk and Microstructures* (Oxford: Oxford University Press)

[144] Kwong N H, Rupper G and Binder R 2009 Self-consistent T-matrix theory of semiconductor light-absorption and luminescence *Phys. Rev.* B **79** 155205
[145] van Roosbroeck W and Shockley W 1954 Photon-radiative recombination of electrons and holes in germanium *Phys. Rev.* **94** 1558–60
[146] Hasselbeck M P, Sheik-Bahae M and Epstein R I 2007 Effect of high carrier density on luminescence thermometry in semiconductors *Proc. SPIE Laser Cooling of Solids (San Jose, CA)* p 646107
[147] Imangholi B, Hasselbeck M P, Sheik-Bahae M, Epstein R I and Kurtz S 2005 Effects of epitaxial lift-off on interface recombination and laser cooling in GaInP/GaAs heterostructures *Appl. Phys. Lett.* **86** 81104
[148] Imangholi B 2006 Investigation of laser cooling in semiconductors *PhD Dissertation* University of New Mexico, Albuquerque, NM
[149] Imangholi B, Hasselbeck M, Bender D, Wang C, Sheik-Bahae M, Epstein R and Kurtz S 2006 Differential luminescence thermometry in semiconductor laser cooling *Proc. SPIE* **6115** 61151C
[150] Sheik-Bahae M, Imangholi B, Hasselbeck M P, Epstein R I and Kurtz S 2006 Advances in Laser Cooling of Semiconductors *Proc. SPIE* **6115** 611518
[151] Li D, Zhang J, Wang X, Huang B and Xiong Q 2014 Solid-state semiconductor optical cryocooler based on CdS nanobelts *Nano Lett.* **14** 4724–8
[152] Imangholi B, Hasselbeck M P and Sheik-Bahae M 2003 Absorption spectra of wide-gap semiconductors in their transparency region *Opt. Commun.* **227** 337–41
[153] Zhang Q, Liu X, Utama M I B, Xing G, Sum T C and Xiong Q 2016 Phonon-assisted anti-stokes lasing in ZnTe nanoribbons *Adv. Mater.* **28** 276–83
[154] Sun G, Chen R, Ding Y J and Khurgin J B 2015 Upconversion due to optical-phonon-assisted anti-stokes photoluminescence in bulk GaN *ACS Photonics* **2** 628–32
[155] Symonds G, Farfan B G, Ghasemkhani M R, Albrecht A R, Sheik-Bahae M and Epstein R I 2016 Thermal management and design for optical refrigeration *Proc. SPIE* **9765** 97650N
[156] Epstein R I, Hehlen M P, Sheik-Bahae M and Melgaard S D 2014 Optical Cryocoolers for Sensors and Electronics *Proc. SPIE* **9070** 90702K
[157] Adams A and Rittenberg E 2014 ADVANCES IN DETECTORS: HOT IR sensors improve IR camera size, weight, and power *Laser Focus World* online
[158] Dhar N K, Dat R and Sood A K 2013 *Advances in Infrared Detector Array Technology Optoelectronics—Advanced Materials and Devices* ed S Pyshkin (InTech) ch 7
[159] Upp D L, Keyser R M, Twomey T R, Keyser R M and Upp D L 2005 New cooling methods for HPGE detectors and associated electronics *J. Radioanal. Nucl. Chem.* **264** 121–6
[160] Kessler T *et al* 2012 A sub-40 mHz-linewidth laser based on a silicon single-crystal optical cavity *Nat. Photon.* **6** 687–92
[161] Kühlbrandt W 2014 The resolution revolution *Science* **343** 1443–4
[162] Cao H S, Witvers R H, Vanapalli S, Holland H J, ter Brake H J M, Holland H J, Vanapalli S, Witvers R H and Cao H S 2013 Cooling a low noise amplifier with a micromachined cryogenic cooler *Rev. Sci. Instrum.* **84** 105102
[163] Hehlen M P 2010 Crystal-Field Effects in Fluoride Crystals for Optical Refrigeration *Proc. SPIE* **7614** 761404